

**Investigation of Solvent Effects on the Hydrodeoxygenation
of Guaiacol over Ru Catalysts**

Journal:	<i>Catalysis Science & Technology</i>
Manuscript ID	CY-ART-09-2019-001763.R1
Article Type:	Paper
Date Submitted by the Author:	01-Oct-2019
Complete List of Authors:	Saleheen, Mohammad; University of South Carolina, Chemical Engineering; Mr. Verma, Anand; University of South Carolina, Chemical Engineering Mamun, Osman; Stanford University Lu, Jianmin; Dalian Institute of Chemical Physics, Chinese Academy of Sciences, Heyden, Andreas; University of South Carolina, Chemical Engineering

24 Abstract

25 The effects of a liquid phase environment on the hydrodeoxygenation of guaiacol, a
26 prototypical lignin derived compound, have been investigated over a Ru catalyst from first
27 principles. A microkinetic reactor model with parameters obtained from density functional theory
28 and implicit solvation schemes was developed to study the effects of condensed phases on the
29 reaction mechanism and kinetic parameters. Phenol was found to be the major aromatic product
30 across all reaction environments. Our model predicts that less protic solvents such as 1-butanol,
31 diethyl ether, and n-hexane have a positive effect on the reaction kinetics for the production of
32 phenolics relative to vapor and aqueous reaction environments. The dominant reaction mechanism
33 for aromatics production remains unchanged across all reaction media. Next, we investigated the
34 possibility of cycloalkane production through hydrogenation of phenol in vapor and liquid phase
35 environments. Our calculations indicated that the reaction pathway for cycloalkane production
36 from phenol will most likely follow an initial dehydrogenation of the hydroxyl group. Based on
37 the vapor phase density functional theory calculations, we proposed a probable reaction pathway
38 and calculated the condensed phase effects along this reaction route. We observed that an aqueous
39 phase has a more favorable effect for cycloalkane production from phenol relative to vapor phase
40 and other less protic solvent environments.

41
42 **Keywords:** Solvent effects; Guaiacol; Phenol; Hydrodeoxygenation; Microkinetic modeling;
43 Density functional theory; Ruthenium

44

45 1. Introduction

46 The discourse about the feasibility and the economic viability of utilizing biomass as an
47 alternative energy source to produce biofuels has intensified lately.¹ Despite the sustainability and
48 the environmental friendliness of this renewable resource, the over reliance of the existing
49 technologies on food grade biomass resources poses some significant challenges.²⁻³ Therefore,
50 upgrading of lignocellulosic biomass to second generation liquid transportation fuels has been
51 receiving widespread attention.⁴⁻⁶ Thermochemical conversion processes such as flash pyrolysis
52 or hydrothermal liquefaction can be employed to produce environmentally benign bio-oils from
53 these biomass sources. Bio-oils have higher energy density and better transportability than
54 feedstock biomass and can generate CO₂ and SO_x credits with lower NO_x emissions compared to
55 fossil fuels.⁷ Dependent on the biomass sources and the conversion processes adopted, the oxygen
56 content in bio-oils can approach as high as 50%, despite having low sulfur and nitrogen content in
57 comparison to fossil-based oils.⁸⁻⁹ The presence of a large oxygen content combined with corrosive
58 acids and reactive aldehydes in the complex bio-oil mixture leads to several undesirable properties,
59 such as low heating value, high viscosity, non-volatility, thermal instability, high degree of
60 corrosiveness, and tendency to polymerize upon exposure to air⁹ which limits the prospect of direct
61 substitution of bio-oils for petroleum fuels. Therefore, some upgrading processes need to be
62 employed to reduce the O/C ratio of the pyrolysis oil for wider range of applications.

63 Catalytic flash pyrolysis and hydrodeoxygenation (HDO) are two of the most promising
64 catalytic upgrading processes for bio-oil. *In-situ* catalytic flash pyrolysis processes have the
65 advantage of being operated at atmospheric pressure in absence of hydrogen;⁷ however, the high
66 degree of oxygen removal and the ability to prevent coke deposition on the catalyst surface have
67 made HDO the more promising alternative.¹⁰ Catalytic HDO of bio-oils is typically performed at

68 high hydrogen pressure to reduce the oxygen content as well as to increase the H/C ratio. Sulfided
69 catalysts such as CoMo and NiMo on γ -Al₂O₃ support have been thoroughly studied for HDO due
70 to their conventional industrial application in the hydrodesulfurization (HDS) of petroleum oils.¹¹⁻
71 ¹³ However, the instability of the sulfided catalysts in presence of sulfur free bio-oils,¹⁴⁻¹⁵ evolution
72 of sulfur containing HDO intermediates owing to the co-feeding of H₂S to maintain the sulfide
73 structure,¹⁶ boehmite formation of the acidic support in presence of water present in the bio-oil
74 mixture,^{15,17} and deactivation of the catalyst surface by polymerization and coke formation¹⁸⁻¹⁹
75 restrict the prospect employing conventional HDS catalysts for HDO purposes. The tendency of
76 bio-oils to thermal degradation and coke formation makes noble metals industrially attractive
77 catalysts despite the higher cost due to their excellent activity, selectivity and stability.^{16,20} They
78 are expected to operate at mild reaction conditions without any introduction of sulfur, and fast
79 deactivation by coke formation in the presence of phenolic compounds can be avoided by
80 employing a high hydrogen pressure during HDO. Nonetheless, further improvement of the
81 catalyst design by tailoring the active phase and the support is required to reduce the hydrogen
82 consumption and increase the yield of selective oils.

83 Bio-oils derived from different feedstocks are typically a complex mixture of water (10-
84 30%) and 300 different organic compounds, comprising of insoluble pyrolytic lignin, aldehydes,
85 organic acids, sugar oligomers, alcohols, and phenol derivatives.²¹ Guaiacyl species, being the
86 primary structure of lignin, are predominant in bio-oils and tend to repolymerize to form coke and
87 heavy hydrocarbons during bio-oil upgrading processes.²²⁻²³ The presence of these diverse organic
88 compounds complicates the bio-oil upgrading process which makes the mechanistic investigation
89 of reaction pathways and catalytic activities very challenging. Therefore, for better understanding
90 of the catalytic upgrading process, it is imperative to select a model compound representative of

91 the pyrolysis oil. In the current study, guaiacol (2-methoxyphenol) has been chosen as the
92 prototypical compound of phenol derivatives and lignin derived oligomers which contains a phenyl
93 ring, two different oxygenated functions, and has been known to play a significant role in the
94 catalyst deactivation process. HDO of guaiacol over a wide range of monometallic transition
95 metals such as Pt^{16,24-31}, Rh^{16,26,30,32}, Pd^{16,26,28,30,33-34}, Ru^{26,28,30,33,35-36}, Fe^{28,37}, Mo³³, Ir³³, W³³,
96 Cu^{28,33}; post transition metals such as Sn²⁴ as well as bimetallic catalysts such as Rh-Pd³², Rh-Pt³²,
97 Pt-Sn²⁴, Ni-Cu³⁸, Pd-Fe²⁸ have been reported. Due to the critical role of metal-support interaction,
98 support acidity, susceptibility of conventional γ -Al₂O₃ support to coke formation^{8,39}, and its
99 instability in presence of water^{17,39}; various supports such as C^{26,28,33,35}, ZrO₂^{16,32,38}, TiO₂^{29,35},
100 SiO₂^{26,35,37-38}, CeO₂^{38,40}, MgO^{27,36} have also been tested rigorously. Heeres et al.⁴¹ presented a
101 thorough catalyst screening using noble metals catalysts and compared that with the conventional
102 hydrotreatment catalysts for HDO of fast pyrolysis oil. They addressed Ru/C as the most promising
103 candidate for bio-oil upgrading regarding oil yields, deoxygenation activity, and hydrogen
104 consumption. Our group has previously reported an in-depth vapor phase mechanistic
105 investigation of the HDO of guaiacol over a Ru(0001) model surface and concluded phenol to be
106 the major product.⁴² However, the presence of a substantial amount of water in bio-oil feeds (30%)
107 combined with the production of more water during the HDO process can affect the activity as
108 well as the surface structure and chemical composition of the catalysts.⁹ If used as a solvent, water
109 has the potential to increase the targeted product selectivity, reduce the undesirable thermal
110 degradation, and facilitate product separation. Sharpless et al.⁴³ reported accelerated reaction rates
111 of hydrophobic organic compounds in water and argued that the biphasic boundary between water
112 and hydrophobic oil can also play a role. Conversely, Grunwaldt and coworkers⁴⁴⁻⁴⁵ have

113 investigated how various polar and non-polar solvents influence the HDO of guaiacol over Pt
114 based catalysts and reported a higher HDO ability in presence of non-polar solvents.

115 To address this lack of fundamental understanding of solvent effects, we report herein an
116 investigation of solvent influence on the reaction mechanism and possible activity descriptors for
117 the HDO of guaiacol over a Ru(0001) model surface. Several studies conducted at relatively mild
118 reaction conditions have reported the presence of aromatic ring saturated products^{36,46} which was
119 not considered in our previous study. Therefore, in this study, we have extended our calculations
120 to investigate the formation of phenyl ring saturated products in vapor and condensed phases.
121 While electrostatic interactions and hydrogen bonding contributions are instrumental for the
122 interaction between a polar adsorbate and a polar solvent, London dispersion forces play a crucial
123 part for non-polar adsorbate-solvent systems. To consider both of these effects, four different
124 solvents of varying degree of polarity (dependent on Kamlet and Taft's solvatochromic
125 parameters) have been employed for this study.⁴⁷ Specifically, we focused on the effects of liquid
126 water which is a polar, protic solvent, 1-butanol, a polar aprotic solvent, diethyl ether, a
127 'borderline' polar aprotic solvent, and a non-polar solvent, n-hexane. Using first principles
128 calculations and a novel implicit solvation scheme for solid surfaces (iSMS),⁴⁸ we characterized
129 the solvent effects on the thermodynamics and kinetics of elementary reactions. It should be noted
130 here that hydrogen bonding contributions are implicitly parameterized in the Conductor like
131 Screening Model (COSMO)^{73,74} and that iSMS has been shown to perform reasonably well for
132 neutral species¹⁰⁰ and for reactions when hydrogen bonding contributions do not change
133 significantly along the reaction coordinate.^{50,101} A mean field microkinetic reactor model was then
134 developed to reexamine the most abundant surface intermediates, dominant reaction pathways,
135 and general kinetic trends in the condensed phases. We conclude our findings with a deliberation

136 of our hypotheses and suggest further research. To the best of our knowledge, no theoretical report
137 on solvent effects on the catalytic hydrodeoxygenation of guaiacol over transition metals catalysts
138 has yet been published.

139

140 **2. Computational Approach**

141 **2.1 Solvation Model**

142 Solvent molecules can affect activity and selectivity of a heterogeneously catalyzed
143 reaction in a number of ways, it can 1) compete with the adsorbed moieties for the active catalyst
144 sites, 2) directly involve itself in the reaction coordinate, thereby providing lower energy pathways,
145 for example, Grotthuss mechanism,⁴⁹ and 3) affect the stability of the charged intermediates or
146 transition states. While computational investigations of chemical reactions occurring at solid-
147 liquid interfaces can be very challenging,⁵⁰ in this study, the liquid phase effect has been
148 approximated by employing the iSMS method.⁴⁸ A detailed discussion about the iSMS
149 methodology and validation can be found elsewhere.^{48,50-54}

150 The fundamental idea behind the iSMS methodology is to include long-range metallic
151 interactions through periodic-slab models in the absence of solvent molecules and to represent the
152 liquid phase effect as a perturbation on the (free) energy differences which is described by
153 (sufficiently large) cluster models embedded in an isotropic continuum of constant dielectric.
154 Consequently, the free energy function of a moiety adsorbed on a periodic metal slab submerged
155 in liquid can be illustrated using the following subtraction scheme,

$$156 \quad G_{\text{surface} + \text{intermediate}}^{\text{liquid}} = G_{\text{surface} + \text{intermediate}}^{\text{vacuum}} + (G_{\text{cluster} + \text{intermediate}}^{\text{liquid}} - E_{\text{cluster} + \text{intermediate}}^{\text{vacuum}}) \quad (1)$$

157 where $G_{\text{surface} + \text{intermediate}}^{\text{vacuum}}$ is the free energy of the adsorbed moieties in vapor phase,

158 $G_{\text{cluster} + \text{intermediate}}^{\text{liquid}}$ is the free energy of the surface cluster model immersed in an implicit solvent

159 which is fashioned by extracting selected metal atoms and removing the periodic boundary
160 conditions, and $E_{cluster + intermediate}^{vacuum}$ is the DFT energy of the same cluster in absence of any fluid
161 phase environment, i.e., solvation effects are captured by the term in the bracket of Eq. 1. The
162 Conductor-like Screening Model for Real Solvents (COSMO-RS)⁵⁵ approach using the
163 COSMOtherm program package⁵⁶ has been employed to compute $G_{surface + intermediate}^{liquid}$. Solvent
164 thermodynamic properties are readily available in the COSMOtherm database,⁵⁶ which are based
165 on the quantum chemical COSMO calculations at the BP-TZVP level of theory. For any other
166 adsorbed moiety, the COSMO-RS input file was generated with the help of COSMO calculations
167 at the same level of theory. We note that COSMO-RS is specifically parameterized for the BP-
168 TZVP level of theory.

169 **2.2 Periodic and Non-periodic DFT Calculations**

170 The catalyst model investigated in this study has been explored earlier for the vapor phase
171 hydrodeoxygenation of guaiacol over a Ru(0001) model surface,⁴² and we encourage the interested
172 readers to review the methods section of that article for a comprehensive summary of the
173 computational details employed to perform the periodic plane-wave DFT calculations. However,
174 it has been demonstrated recently that the Bayesian error estimation functional with van der Waals
175 correction (BEEF-vdW)⁵⁷ performs significantly better for calculating the adsorption energies of
176 larger adsorbates⁵⁸⁻⁵⁹ as well as simple adsorbates such as CO⁶⁰⁻⁶¹ in comparison to the PBE
177 functional⁶² with dispersion corrections that we used previously.⁶³ Hence, the energetics of the
178 adsorption-desorption processes as well as the all the elementary steps of the phenol hydrogenation
179 network investigated in this study have been computed utilizing the BEEF-vdW functional. All
180 periodic DFT calculations have been performed using the VASP⁹⁹ program package and non-
181 periodic cluster model DFT calculations have been performed using the TURBOMOLE 6.5⁶⁴⁻⁶⁵

182 program package. The cluster surfaces have been constructed by removing the periodicity of the
183 geometries obtained from plane-wave DFT calculations and modeled as a 5×5 surface with 2 layers
184 of metal atoms which we found to lead to converged solvation effect data with regards to cluster
185 depth and size. Atoms that comprise the adsorbate molecules have been described by employing
186 all electron basis sets of triple- ζ quality,⁶⁶ while a relativistic effective small core potential (ECP)
187 combined with a basis set of the same quality as the adsorbate atoms have been employed for the
188 valence electrons of the metal (Ru) atoms.⁶⁷ Electron exchange and correlation terms of DFT have
189 been described by utilizing the BP86 functional⁶⁸⁻⁶⁹ and coulomb potentials were approximated in
190 conjunction with the RI-J approximation using auxiliary basis sets.⁷⁰⁻⁷¹ Single point energy
191 calculations have been performed for the cluster models using a self-consistent field energy
192 convergence criterion of 1.0×10^{-7} Ha with an m4 spherical grid.⁷² Multiple spin states were
193 investigated for each cluster model to identify the lowest energy spin state. For the lowest energy
194 spin state, Conductor like screening model calculations (COSMO)⁷³⁻⁷⁴ were performed where the
195 solute molecule is embedded in a molecule shaped cavity surrounded by a dielectric medium of
196 infinite dielectric constant (hence Conductor). Finally, the dielectric constant was scaled down to
197 the respective dielectric constant of the solvents by utilizing the COSMO-RS⁵⁶ program package
198 to obtain the solvation energy. Considering the ambiguity associated with the interpretation of the
199 cavity radius of transition metal atoms in implicit solvation models (due to a lack of available
200 experimental data),^{50,75} all calculations have been repeated with a 10% incremental change on the
201 default cavity radius of the Ru atoms.

202 **2.3 Solvents Investigated**

203 The HDO of guaiacol has previously been studied experimentally for the pure reactant
204 diluted in water, diethylether, decane, octanol, hexadecane, and tetrahydrofuran.^{44,76-78} In organic

205 chemistry, it is often attempted to understand solvent effects by the *polarity* of the solvent, which
206 can be very challenging to convey quantitatively. Empirical estimation of solvent polarity has been
207 calculated based on linear free energy relationships of substituent solvent parameters and
208 equilibrium, kinetic, and spectroscopic measurements.⁴⁷ By employing a solvatochromic
209 comparison method in linear solvation energy relationship (LSER) theory, Kamlet and Taft
210 presented a set of solvent parameters to establish a solvent polarity scale, namely, π^* , α , and β ,
211 which are related to distinct configurational properties in solution, e.g., solubilities, partition
212 coefficients, thermodynamic and kinetic properties of chemical reactions, etc.⁷⁹⁻⁸¹ They correlated
213 solvent dependent physicochemical properties of a given solvent and a reference solvent by
214 introducing some solvent independent coefficients (s , a , b) which specify the susceptibility of the
215 corresponding parameters, dipolarity/polarizability (π^*), hydrogen-bond donor acidities (α), and
216 hydrogen-bond acceptor basicities (β), respectively. Table-S1 in the supporting information
217 includes the Kamlet-Taft solvent parameters as well as the normalized solvent polarity parameter
218 (E_T^N) for the four different solvents explored in this study, i.e., water, 1-butanol, diethylether, and
219 n-hexane. The recorded values clearly indicate that water is the most polar protic solvent with high
220 polarizability and hydrogen bond donating ability while n-hexane lies at the other end of the
221 spectrum with no hydrogen bond accepting/donating capability. 1-butanol and diethylether lie in
222 between the above mentioned two as evidenced from their normalized polarity values.

223

224 **3. Model Development**

225 **3.1 Microkinetic Modeling**

226 To analyze the implication of reaction energies and the reaction pathways under realistic
227 processing conditions, a mean-field microkinetic model was formulated. The formulation of the

228 partition function in the liquid phase environment is complex and dynamic contributions to the
 229 free energy of the solute are in general insensitive to whether the solute vibrational frequencies are
 230 computed in the gas phase or in the solution. Thus, in the parameterization of implicit solvation
 231 models, the vibrational partition function is often computed for the gas phase species. Hence, the
 232 zero-point corrections to the 0 K energies and vibrational partition functions under the harmonic
 233 approximation were calculated using the vibrational frequencies (ν_i) obtained from vapor phase
 234 periodic plane-wave DFT calculations.

$$E_{ZPE} = \frac{1}{2} \sum_i h\nu_i \quad (2)$$

$$q_{vib} = \prod_i \frac{1}{1 - \exp\left(-\frac{h\nu_i}{k_B T}\right)} \quad (3)$$

235 It should be noted here that the frequency calculations include relaxations of only adsorbed
 236 moieties which result in a reduction of the accuracy of low-lying frequencies that are coupled with
 237 surface metal atoms. Considering the accuracy of DFT (or lack thereof) and the inadequacy of the
 238 harmonic approximation to describe low-lying frequencies, we established a 100 cm^{-1} cutoff value
 239 for frequencies (real) that lie below the aforementioned value. This accommodation was not
 240 required for the gas phase molecules since the rotational and the vibrational partition functions
 241 were rigorously calculated using statistical mechanics.⁸²

242 To account for the liquid phase environment, the solvation free energy obtained from
 243 COSMO-RS calculations were utilized to reparametrize the microkinetic model. For the
 244 adsorption/desorption processes,

$$\Delta G_{solvent} = \Delta G_{gas} + G_{ads}(solv) - G_{Ru}(solv) \quad (4)$$

245 where $G_{ads}(solv)$ and $G_{Ru}(solv)$ are the free energies of solvation of a Ru cluster with and without
 246 an adsorbate, respectively. It is worth mentioning here that the chemical potential of all the gas

247 phase species in a particular solvent is given by the partial pressure (fugacity) of that species in
 248 the vapor phase which is in equilibrium with the solvent phase, i.e., we assumed gas-liquid
 249 equilibrium in the absence of any mass transfer limitations. The free energy of reaction ($\Delta G_{solvent}^{rxn}$)
 250 and free energy of activation ($\Delta G_{solvent}^{\ddagger}$) of the elementary surface reactions were calculated as,

$$\Delta G_{solvent}^{rxn} = \Delta G_{gas}^{rxn} + G_{FS}(solv) - G_{IS}(solv) \quad (5)$$

$$\Delta G_{solvent}^{\ddagger} = \Delta G_{gas}^{\ddagger} + G_{TS}(solv) - G_{IS}(solv) \quad (6)$$

251 where the subscripts IS, TS, and FS denote the initial, transition, and final state, respectively. All
 252 reactions were presumed to be reversible reactions. Forward rate constants were calculated using
 253 harmonic transition state theory (hTST)⁸³ for all surface mediated elementary processes.

$$k_{forward} = \frac{\gamma k_B T}{h} \exp\left(\frac{-\Delta G^{\ddagger}}{k_B T}\right) \quad (7)$$

254 Here, ΔG^{\ddagger} is the free energy of activation, T is the absolute temperature, γ is the transmission
 255 coefficient, which was assumed to be 1.0 for all cases, and k_B and h are the Boltzmann and Planck
 256 constants, respectively. Collision theory was employed for calculating the forward rate constants
 257 of non-activated adsorption processes.

$$k_{forward} = \frac{\sigma}{N_o \sqrt{2\pi m k_B T}} \quad (8)$$

258 Here, σ stands for the sticking probability (assumed to be 1.0 for all cases), N_o is the number of
 259 catalytic sites per unit surface area, and m is the molecular weight of the adsorbate.
 260 Thermodynamic consistency was ensured by calculating the reverse rate constants from
 261 thermodynamic equilibrium constants.

$$K_{eq} = \exp\left(\frac{-\Delta G^{rxn}}{k_B T}\right) \quad (9)$$

$$k_{reverse} = \frac{k_{forward}}{K_{eq}} \quad (10)$$

262 Finally, with all the rate parameters known, a microkinetic reactor model was developed as a
263 system of differential algebraic equations (DAEs). The fractional coverage of a surface
264 intermediate at steady state is given by,

$$\frac{d\theta_i}{dt} = \sum_j \nu_{i,j} r_j = 0 \quad (11)$$

265 where index i refers to the i th adsorbed species and index j loops over all the elementary reactions.
266 Furthermore, the total number of catalytic sites were conserved, and the overall site balance
267 equation was employed to calculate the fractional coverage of empty sites.

$$\sum_i n_i \theta_i = 1 \quad (12)$$

268 A complete list of the number of sites assigned to each species (n_i) can be found in our vapor phase
269 study.⁴² All microkinetic models were initialized with a clean Ru surface and solved as a system
270 of DAEs to achieve fractional surface coverages and turnover frequencies (TOFs) at steady state
271 under realistic processing conditions.

272 3.2 Adsorbate-adsorbate Interactions

273 Adsorbate-adsorbate interactions can play a significant role for the adsorption strength as
274 well as the stability of the adsorbed moieties which in turn can affect catalytic activity of transition
275 metal catalysts.^{54,75,84-85} Getman et al.⁸⁶⁻⁸⁷ demonstrated a remarkable change in NO_2 dissociation
276 capability of Pt(111) when the O coverage is typical for NO oxidation catalysts. As reported in our
277 vapor phase study,⁴² without considering any adsorbate-adsorbate interactions, H , CO , and
278 phenoxy (C_6H_5O) become the most abundant surface intermediates when solving the microkinetic
279 modeling equations. Hence, to mimic the local chemical environment dependence of adsorption
280 energy in a realistic reaction environment, lateral interaction functional forms have been included
281 in our microkinetic model. While the true description of adsorbate-adsorbate interactions can be

282 very complicated and computationally demanding to realize, we employed the two-parameter
283 lateral interaction model proposed by Grabow et al.⁸⁸ considering its simplicity. Table S2 of the
284 supporting information includes the functional forms of the lateral interactions introduced in our
285 microkinetic models. A detailed description of the calculation procedure to obtain these functional
286 forms have been discussed in our vapor phase investigation.⁴²

287

288 **4. Results and Discussion**

289 Experimental studies have reported a range of alicyclic and aromatic products for the HDO
290 of guaiacol such as 2-methoxy-cyclohexanol, cyclohexanol, cyclohexanone, cyclohexane,
291 benzene, catechol etc. with phenol being a major intermediate detected at short reaction
292 times.^{28,30,33,36,46} Therefore, in this study, we aim to describe the HDO of guaiacol over Ru(0001)
293 catalysts in two steps. At first, we carried out our study in condensed phase to verify the formation
294 of phenol from the hydrodeoxygenation of guaiacol. Next, we examine the possibility of phenyl
295 ring saturation in vapor and condensed phases to produce two major products observed in
296 experimental studies, cyclohexanol and cyclohexanone from phenol.^{78,89-92}

297

298 **4.1 HDO of Guaiacol to Unsaturated Aromatics**

299 **4.1.1 Solvent Effects on the Adsorption Strength of Reaction Intermediates**

300 The introduction of a solvent using a continuum solvation model can alter the adsorption
301 strength of reaction intermediates in two different ways, i) incorporating an implicit solvent
302 introduces the previously unaccounted for adsorbate-solvent interaction, and ii) it modifies the
303 metal-adsorbate interaction by changing the electronic structure of the metal due to indirect
304 solvent-metal interactions. Solvent induced changes in the adsorption strength of a reaction

305 intermediate can significantly affect the overall activity of a catalyst site by modifying the
 306 activation and reaction free energies. To investigate the effects of solvent on the adsorption
 307 strength of the intermediates involved in the HDO of guaiacol, we computed the difference in
 308 adsorption free energy in the absence and presence of a solvent,



$$\begin{aligned} \Delta(G_{ads,A}) &= G_{ads,A}(l) - G_{ads,A}(g) \\ &= [G^{A*}(l) - G^{A*}(g)] - [G^*(l) - G^*(g)] = \Delta(\Delta G) \end{aligned} \quad (15)$$

309 where, $G_{ads,A}(l)$ and $G_{ads,A}(g)$ are the free energies of adsorption of a gas molecule of intermediate
 310 A in the presence and absence of the solvent, $G^{A*}(l)$ and $G^{A*}(g)$ are the free energies of the
 311 adsorbed moiety A in the presence and absence of solvent, and $G^*(l)$ and $G^*(g)$ are free energies
 312 of the clean surface model in the presence and absence of solvent, respectively. It should be noted
 313 here that while many adsorbed moieties can be unstable when separated from their adsorption site;
 314 nonetheless, this scheme permits us to compare the relative adsorption strength in a liquid phase
 315 environment with respect to the gas phase adsorption strength. Using this procedure, we essentially
 316 use an ideal gas phase as reference state for all species and assume equilibrium between the
 317 molecules in the liquid phase and a hypothetical gas phase, i.e., we are assuming fast mass transfer.
 318 The activity coefficient/fugacity of the molecules in the liquid phase at a given concentration in
 319 the various solvents is computed using COSMOtherm.

320 The investigated surface moieties in the reaction network of the HDO of guaiacol and the
 321 calculated change in their adsorption strength in various reaction environments are listed in Table
 322 1. In total, we investigated 39 surface intermediates in our reaction network that includes guaiacol,
 323 phenol, catechol, and their derivatives. Snapshots of all adsorbed geometries can be found in our
 324 previous vapor phase study.⁴² For the convenience of comparison of the solvent effect on the

325 adsorption strength of the surface intermediates, we classified the intermediates into four different
326 classes of structurally similar species where all the species belonging to a class display similar
327 trends in solvent effects across all four solvents studied in this paper.

328 *Class I: Guaiacol and Its Derivatives*

329 Presence of a liquid-phase environment significantly stabilizes the adsorption of guaiacol
330 on Ru(0001) sites ($\Delta(\Delta G^{water}) = -0.22 \text{ eV}$, $\Delta(\Delta G^{1-butanol}) = -0.47 \text{ eV}$, $\Delta(\Delta G^{diethylether})$
331 $= -0.43 \text{ eV}$, $\Delta(\Delta G^{n-hexane}) = -0.33 \text{ eV}$). Solvents employed in this study can be arranged in
332 the order of their effect on the adsorption strength of guaiacol and its dehydrogenated and partially
333 hydrogenated derivatives as 1-Butanol > Diethyl ether > n-Hexane > Water. This phenomenon can
334 be attributed to the fact that guaiacol has a large non-polar aromatic ring with a polar hydroxyl
335 group and slightly polar methoxy group. The presence of a polar solvent (Water) ensures favorable
336 solute-solvent interaction, i.e., formation of hydrogen bonds, thereby increasing the adsorption
337 strength of guaiacol and its derivatives. Reducing the polarity of the solvent (1-Butanol, Diethyl
338 ether) enhances the stabilization of the adsorption strength of these species because of the
339 additional favorable interaction between non-polar fragments of the solute and solvent due to
340 increased London forces while retaining some of the favorable interaction between polar fragments
341 of the solute and solvent. For non-polar aprotic solvents such as n-hexane, the stabilization of the
342 adsorption strength only comes from the favorable solute-solvent interaction due to London
343 dispersion forces, which reduces the solvent effect on the adsorption strength of guaiacol and its
344 derivatives compared to that of 1-butanol and diethyl ether. Partially hydrogenated
345 ($C_6H_4H_{\alpha/\beta}(OH)(OC_xH_y)$), $x=[0,1]$, $y=[0,3]$) and dehydrogenated ($C_6H_4(O_vH_w)(O_xC_yH_z)$), $v=[0,1]$,
346 $w=[0,1]$, $x=[0,1]$, $y=[0,1]$, $z=[0,3]$) species of guaiacol all maintain the same order of the solvent
347 effect on the adsorption strength. For example, the 2-methoxy-phenyl ($C_6H_4(OCH_3)$) intermediate

348 can be produced by $C_{\text{aryl}(\alpha)}\text{-OH}$ bond scission of guaiacol. Due to the loss of a polar hydroxyl
 349 group, the solvent stabilization of the adsorption strength in water gets reduced ($\Delta(\Delta G^{\text{water}})$
 350 $= -0.07 \text{ eV}$) compared to that of guaiacol, while the increasingly non-polar solvents such as 1-
 351 butanol, diethyl ether and n-hexane retain most of the solvent stabilization ($\Delta(\Delta G^{1-\text{butanol}})$
 352 $= -0.35 \text{ eV}$, $\Delta(\Delta G^{\text{diethylether}}) = -0.33 \text{ eV}$, $\Delta(\Delta G^{n-\text{hexane}}) = -0.24 \text{ eV}$) that is due to dispersion
 353 forces between non-polar fragments of the solute and solvent.

354 *Class II: Phenol, Anisole, Catechol, Benzene and Their Derivatives*

355 Phenol, due to the presence of a strongly polar hydroxyl group, displays a significant
 356 solvent stabilization in aqueous phase ($\Delta(\Delta G^{\text{water}}) = -0.20 \text{ eV}$), and the presence of a non-polar
 357 aromatic ring ensures an increase in adsorption strength for other solvents with various degree of
 358 polarity ($\Delta(\Delta G^{1-\text{butanol}}) = -0.38 \text{ eV}$, $\Delta(\Delta G^{\text{diethylether}}) = -0.35 \text{ eV}$, $\Delta(\Delta G^{n-\text{hexane}})$
 359 $= -0.26 \text{ eV}$). On the other end of the spectrum, benzene, being non-polar, shows a small solvent
 360 stabilization in its adsorption strength in the aqueous phase ($\Delta(\Delta G^{\text{water}}) = -0.10 \text{ eV}$). However,
 361 benzene shows a sizable solvent stabilization in adsorption strength in the other solvents due to
 362 favorable solute-solvent London dispersion interaction ($\Delta(\Delta G^{1-\text{butanol}}) = -0.26 \text{ eV}$, Δ
 363 $(\Delta G^{\text{diethylether}}) = -0.24 \text{ eV}$, $\Delta(\Delta G^{n-\text{hexane}}) = -0.17 \text{ eV}$). Overall, phenol ($\text{C}_6\text{H}_5\text{OH}$), anisole
 364 ($\text{C}_6\text{H}_5\text{OCH}_3$), catechol ($\text{C}_6\text{H}_4(\text{OH})_2$), benzene (C_6H_6), and their dehydrogenated surface
 365 intermediates follow the same order of solvent stabilization as mentioned before for guaiacol
 366 species.

367 *Class III: Methane and Its Derivatives*

368 Methane and its dehydrogenated derivatives such as methyl (CH_3), methylene (CH_2), and
 369 methylidyne (CH) display a marginally weaker adsorption strength in the aqueous phase due to
 370 their non-polar nature. For example, the adsorption strength of methane in liquid water decreased

371 by 0.04 eV. We also find that the adsorption strength of methane and its derivatives is hardly
372 affected by the presence of other solvents such as 1-butanol, diethyl ether, and n-hexane.

373 *Class IV: Methanol and Its Derivatives*

374 Presence of liquid water weakens the adsorption strength of strongly polar methanol and
375 its dehydrogenated species methoxy (CH_3O) ($\Delta(\Delta G_{\text{methanol}}^{\text{water}}) = 0.12 \text{ eV}$, $\Delta(\Delta G_{\text{methoxy}}^{\text{water}}) = 0.09 \text{ eV}$
376). This inverse solvent effect on a polar species can be rationalized by observing their binding
377 modes and their strongly polar nature. Both methanol and methoxy species binds to the Ru(0001)
378 surface through the O atom, a hydrogen bond donor. Due to their polar nature, these species have
379 a favorable solute-solvent interaction in polar solvents (through hydrogen bonding) which in turn
380 weakens solute-surface interaction, thereby reducing the adsorption strength when following bond
381 order conservation principles. As we decrease the polarity of the solvents, the adsorption strength
382 gets stabilized. For less polar dehydrogenated species such as formaldehyde (CH_2O) and formyl
383 (CHO), the presence of a liquid phase environment hardly affects the adsorption strength.

384 **4.1.2 Solvent Effects on Elementary Processes**

385 Figure 1 illustrates a schematic of the investigated elementary reactions involved in the
386 HDO of guaiacol over a Ru(0001) model surface. Energetics of all adsorption/desorption reactions
387 are reported in Table 2 using BEEF-vdW functional in different reaction environments at 473 K.
388 Free energies of reaction and free energies of activation of all elementary surface processes in
389 different reaction environments are listed in Table 3 for a reaction temperature of 473 K.

390 In the following, we discuss the solvent effects on the free energy of reaction and free
391 energy of activation of various elementary processes involved in the HDO of guaiacol. For the
392 convenience of comparison, the reaction pathways have been labeled from 2 to 8 according to the
393 first reaction step labeled in Figure 1, adsorption of guaiacol being the first reaction step. Pathways

394 2 and 3 start with selective hydrogenation of $C_{\text{aryl}(\beta)}$ and $C_{\text{aryl}(\alpha)}$ of guaiacol, respectively. Direct
 395 removal of a hydroxyl group, methoxy group, and a methyl group from guaiacol have been
 396 considered in pathways 4, 5, and 7, respectively. Pathways 6 and 8 considers the dehydrogenation
 397 of guaiacol through C-H bond scission of the methoxy group and O-H bond scission of the
 398 hydroxyl group, respectively.

399 *I: Selective hydrogenation of the phenyl ring*

400 Selective hydrogenation of the phenyl ring of guaiacol to form $C_6H_4H_\beta(OH)(OCH_3)$ (step
 401 2) and $C_6H_4H_\alpha(OH)(OCH_3)$ (step 3) are both endergonic steps in the vapor phase ($\Delta G_{rxn} = 0.40$ eV
 402 and $\Delta G_{rxn} = 0.51$ eV, respectively) and kinetically demanding with a free energy of activation of
 403 1.10 eV and 1.14 eV, respectively, which makes pathways 2 and 3 unfavorable. Liquid solvents
 404 employed in this study (water, 1-butanol, diethyl ether, and n-hexane) have an unfavorable effect
 405 on the free energies of $C_{\text{aryl}(\beta)}$ -H hydrogenation, making it more endergonic (free energy of reaction
 406 ranging from 0.41 eV to 0.49 eV) and making it kinetically more demanding. Liquid water does
 407 not have any effect on the free energy of reaction of $C_{\text{aryl}(\alpha)}$ -H hydrogenation, with a minimal
 408 increase in the free energy of activation ($\Delta(\Delta G^\ddagger) = 0.04$ eV). Employing other solvents such as 1-
 409 butanol, diethyl ether, or n-hexane have a minimal exergonic effect on the free energy of reaction
 410 with a slight increase in the free energy of activation ($\Delta(\Delta G_{1-\text{butanol}}^\ddagger) = 0.06$ eV, $\Delta(\Delta G_{\text{diethyl ether}}^\ddagger)$
 411 $) = 0.06$ eV, $\Delta(\Delta G_{\text{n-hexane}}^\ddagger) = 0.07$ eV).

412 Similar to the vapor phase, further dehydrogenation of the methoxy group (step 9) remains
 413 challenging compared to the methoxy group removal (step 10) of $C_6H_4H_\beta(OH)(OCH_3)$ in all
 414 solvents studied. Liquid water increases the free energy of activation of the subsequent methylene
 415 group removal (step 23) process by 0.16 eV while it remains largely unaffected in all other solvent
 416 media. The energetics of the hydrogenation of the resulting $C_6H_4H_\beta(OH)(O)$ species to produce

417 $C_6H_5(OH)_2$ (step 36) also show only a minimal perturbation from the vapor phase for different
418 solvent media. The final step to produce phenol involves dehydroxylation of the phenyl ring (step
419 41) and employing increasingly non-polar solvents makes this step more facile by 0.11-0.15 eV.

420 Less protic solvent media such as 1-butanol, diethyl ether, and n-hexane have an
421 endergonic effect on the free energy of activation for the dehydroxylation of the $C_{aryl}(\alpha)$
422 hydrogenated species of guaiacol (step 11) to produce anisole while the energetics remain
423 unchanged in water compared to that of vapor phase. Different reaction media also exert a limited
424 effect on the kinetics of the subsequent dehydrogenations of anisole (step 24 and step 37). Overall,
425 the energetics of pathways 2 and 3 suggest that HDO of guaiacol does not proceed through
426 selective hydrogenation of the phenyl ring, similar to the vapor phase, which agrees with
427 experimental observations.²⁸

428 *II: Direct removal of functional groups*

429 Pathways 4, 5, and 7 consider direct removal of -OH, -OCH₃, and -CH₃ functional groups,
430 which were found to be kinetically difficult in the vapor phase and which remain difficult in liquid
431 phase environments. A liquid phase environment exerts an endergonic effect on the
432 thermodynamics of the removal of the hydroxyl species from guaiacol to produce 2-methoxy
433 phenyl species ($C_6H_4OCH_3$) (step 4). While the presence of an aqueous phase increases the free
434 energy of activation by 0.07 eV, other solvent media hardly affect the kinetics of the reaction.
435 Subsequent hydrogenation to anisole, however, gets more exergonic in the liquid phase
436 environment with water contributing the most $\Delta(\Delta G_{rxn}) = -0.22 eV$ while the kinetics also
437 become slightly facilitated.

438 In the methoxy group removal pathway (pathway 5), the removal of the -OCH₃ species
439 (step 5) becomes kinetically more unfavorable in water ($\Delta(\Delta G^\ddagger) = 0.07 eV$) while other solvents

440 have a minimal effect. Subsequent hydrogenation of the 2-hydroxy phenyl species (C_6H_4OH) to
441 produce phenol (step 13) becomes thermodynamically more favorable in the liquid phase
442 environment compared to that of the vapor phase.

443 The seventh pathway consists of removal of a methyl group from guaiacol to produce a
444 hydrogen catecholate species ($C_6H_4(OH)(O)$) (step 7) which is highly exergonic in the vapor phase
445 ($\Delta G_{rxn} = -1.35 eV$). Introduction of a liquid phase environment has an endergonic effect on the
446 thermodynamics of the reaction while the kinetics remains mostly unchanged. The hydrogen
447 catecholate can be hydrogenated to catechol (step 18) which remains largely unchanged in liquid
448 water, while less protic solvents have a favorable effect on both the thermodynamics and the
449 kinetics of this elementary process. Catechol can be either dehydroxylated to a 2-hydroxy phenyl
450 species (C_6H_4OH) (step 27) or hydrogenated to produce a $C_6H_5(OH)_2$ species (step 28) which are
451 both kinetically very demanding. Presence of a liquid phase environment does not affect the
452 kinetics of these processes while having minimal effect on the thermodynamics.

453 In summary, a liquid phase environment does not help these kinetically demanding
454 processes of direct functional group removal to make them more facile.

455 *III: Dehydrogenation of methoxy and hydroxyl groups*

456 In pathways 6 and 8, we discuss the initial dehydrogenation of the $-OCH_3$ and $-OH$ groups
457 of guaiacol. The removal of a hydrogen from the methoxy group of guaiacol to produce the 2-
458 methylene-oxy-phenol intermediate ($C_6H_4(OH)(OCH_2)$) (step 6) is both thermodynamically and
459 kinetically favorable in the vapor phase ($\Delta G_{rxn} = -0.36 eV$, $\Delta G^\ddagger = 0.50 eV$). Introduction of an
460 aqueous phase has an endergonic effect on the free energy of reaction ($\Delta(\Delta G_{rxn}) = 0.09 eV$) with
461 negligible impact on the free energy of activation ($\Delta(\Delta G^\ddagger) = 0.02 eV$). All the other less protic
462 solvents (1-butanol, diethyl ether, and n-hexane) have a less endergonic effect on the

463 thermodynamics of the reaction compared to water ($\Delta(\Delta G_{rxn}) = 0.04 \text{ eV}$) with the kinetics
464 remaining unperturbed. 2-methylene-oxy-phenol species can go through $-\text{OCH}_2$ removal (step 14),
465 dehydrogenation at the hydroxyl group (step 15), dehydrogenation of the methylene group (step
466 16), and removal of $-\text{CH}_2$ (step 17). The most facile path in the vapor phase is dehydrogenation of
467 the methylene group (step 16) ($\Delta G_{rxn} = -0.53 \text{ eV}$, $\Delta G^\ddagger = 0.02 \text{ eV}$), which remains unchanged in
468 the liquid phase environment. However, while the liquid phase environment does not affect the
469 free energy of reaction of this elementary step, the free energy of activation is perturbed differently
470 for polar and non-polar solvents. The reaction becomes barrierless in an aqueous phase while for
471 other solvents, the free energy of activation increases by 0.10 eV compared to that of the vapor
472 phase. The product of step 16, 2-methylidyne-oxy-phenol ($\text{C}_6\text{H}_4(\text{OH})(\text{OCH})$) can then either
473 undergo methyne ($-\text{CH}$) removal to produce a once hydrogenated catecholate intermediate
474 ($\text{C}_6\text{H}_4(\text{OH})\text{O}$) (step 26) or formyl ($-\text{OCH}$) removal to produce a 2-hydroxy-phenyl species
475 ($\text{C}_6\text{H}_4\text{OH}$) (step 25). Step 26 is much more facile compared to step 25 in the vapor phase which
476 remains consistent in the presence of a liquid phase environment. However, while liquid water
477 makes the process more exergonic by 0.09 eV, other less protic solvents makes it more endergonic
478 by 0.17 eV compared to that of the vapor phase. Elementary processes involving the $\text{C}_6\text{H}_4(\text{OH})\text{O}$
479 species have already been discussed in the previous section and consequently will not be discussed
480 further.

481 Finally, the pathway eight, which involves dehydrogenation of the hydroxyl group of
482 guaiacol to produce a guaiacolate intermediate ($\text{C}_6\text{H}_4(\text{O})(\text{OCH}_3)$) (step 8) is the most facile reaction
483 pathway in the vapor phase ($\Delta G_{rxn} = -0.77 \text{ eV}$, $\Delta G^\ddagger = 0.29 \text{ eV}$). In the liquid phase, all solvents
484 pose an endergonic effect on the free energy of reaction of this elementary process by $\sim 0.10 \text{ eV}$.
485 The free energy of activation remains unaltered in less protic solvents while liquid water shows an

486 endergonic effect ($\Delta(\Delta G^\ddagger) = 0.08 \text{ eV}$) making this step competitive with the dehydrogenation of
487 the methoxy group of guaiacol (step 6). Next, the methoxy group is dehydrogenated (step 22)
488 which is more facile ($\Delta G_{rxn} = -0.32 \text{ eV}$, $\Delta G^\ddagger = 0.53 \text{ eV}$) compared to the alternative step which
489 involves complete removal of the methoxy group (step 21) ($\Delta G_{rxn} = 0.21 \text{ eV}$, $\Delta G^\ddagger = 1.08 \text{ eV}$) in
490 the vapor phase. Liquid water further facilitates the kinetics of the methoxy group dehydrogenation
491 step (step 22) ($\Delta(\Delta G^\ddagger) = -0.06 \text{ eV}$). The product of step 22, 2-methylene-oxy-phenolate
492 ($\text{C}_6\text{H}_4(\text{O})(\text{OCH}_2)$) then undergoes a barrierless dehydrogenation reaction (step 33) across all
493 reaction environments to produce a 2-methylidyne-oxy-phenolate ($\text{C}_6\text{H}_4(\text{O})(\text{OCH})$) species where
494 the thermodynamics of the process becomes slightly exergonic (by $\sim 0.05 \text{ eV}$) when using less
495 protic solvents compared to that of the vapor phase. In the vapor phase, two kinetically competing
496 reactions develop at this point, methylidyne (-CH) removal (step 34) and hydrogen removal (step
497 35) from the $\text{C}_6\text{H}_4(\text{O})(\text{OCH})$ intermediate. In the liquid phase environment, the reactions become
498 even more competitive, i.e., the difference between the free energy of activation of these two
499 elementary processes in 1-butanol solvent is only 0.07 eV . The product of step 34, a catecholate
500 species ($\text{C}_6\text{H}_4\text{O}_2$) then undergoes hydrogenation (step 42) which connects the eighth pathway with
501 the sixth at this point. The product of the other elementary step (step 35), 2-carbide-oxy-phenolate
502 ($\text{C}_6\text{H}_4(\text{O})(\text{OC})$), then goes through decarbonylation (step 43) to produce a 2-oxyphenyl ($\text{C}_6\text{H}_4\text{O}$)
503 intermediate. While the kinetics of this reaction mostly remains unperturbed due to the presence
504 of a liquid phase, the free energy of reaction becomes more endergonic ($\Delta(\Delta G_{rxn}) = 0.21 \text{ eV}$) in
505 liquid water while other less protic solvents makes this process more exergonic ($\Delta(\Delta G_{rxn})$
506 $) = -0.08 \text{ eV}$). Lastly, the $\text{C}_6\text{H}_4\text{O}$ species gets hydrogenated to phenol ($\text{C}_6\text{H}_5\text{OH}$) (step 30) and an
507 aqueous phase environment facilitates this process both thermodynamically ($\Delta(\Delta G_{rxn})$
508 $) = -0.12 \text{ eV}$) and kinetically ($\Delta(\Delta G^\ddagger) = -0.09 \text{ eV}$).

509 Based on the thermodynamics and kinetics of the elementary processes, we can presume
510 that the dominant reaction pathway of the vapor phase (pathway 8) remains dominant in all
511 condensed phase reaction media. However, any computational catalysis study based on only free
512 energies remains inadequate for not considering the realistic reaction conditions and not predicting
513 the experimental observables to which it can be compared directly. Therefore, in the following
514 sections, we investigate the effect of solvents on the turn-over frequency (TOF) and the coverage
515 of the most abundant surface intermediates through mean-field microkinetic modeling.

516 4.1.3 Mean-field Microkinetic Modeling

517 In our previous study, we investigated the vapor phase kinetics of the HDO of guaiacol
518 over a Ru(0001) surface⁴² where we found that at low hydrogen partial pressure and moderate
519 reaction temperature (573K), kinetically the most favorable pathway proceeds through
520 dehydrogenation of the hydroxyl group of guaiacol (pathway 8) and the major reaction product
521 was phenol with catechol as the most relevant side product. In this study, we extend our
522 microkinetic model to account for the effect of solvation by including the change in free energy of
523 reaction and free energy of activation due to the presence of a condensed phase. We utilized the
524 experimental reaction conditions of 0.50 g of guaiacol in 10 g of solvent under relatively mild
525 reaction conditions (473 K) and 15 bar partial pressure of H₂, similar to the reaction conditions of
526 Tomishige et al.^{36,46} To find the corresponding fugacity/partial pressure of guaiacol, we utilized
527 the modified Raoult's law,

$$528 \quad f_{gua}^v = P_{gua} = x_{gua}\gamma_{gua}P_{gua}^{sat} \quad (16)$$

529 Thermodynamic data such as activity coefficient, saturation pressure of guaiacol, and fugacity of
530 pure solvent have been calculated using the COSMOtherm program package.⁷³⁻⁷⁴ We calculated
531 the guaiacol fugacity to be 0.94 bar, 0.03 bar, 0.02 bar, and 0.05 bar in liquid water, 1-butanol,

532 diethyl ether, and n-hexane, respectively at 473 K and assuming 1% conversion, the phenol partial
533 pressure was set accordingly. For vapor phase simulations, we used a guaiacol chemical
534 potential/fugacity corresponding to the one in liquid water. Using low conversion conditions to
535 other reaction products such as catechol, anisole, and benzene, their partial pressures were set at
536 10^{-6} bar. We chose a slightly higher partial pressure of CO (10^{-4} bar) to observe the poisoning
537 effect of CO on the reaction mechanism, similar to our prior research.⁴² For all simulations, we
538 employed the same coverage dependent adsorption energies as reported in our previous
539 contribution⁴² for the three most abundant surface intermediates of the vapor phase, H, CO, and
540 phenoxy (C_6H_5O). A summary of our calculated TOFs at four different reaction temperatures and
541 at various reaction environments are presented in Table 4.

542 *I. Liquid Water Effects*

543 In the presence of an aqueous phase at 473 K (i.e., at a corresponding equilibrium water
544 partial pressure of 15.536 bar), we observe that the surface is predominantly covered with CH,
545 CO, H, and phenoxy (C_6H_5O) species (Table 5). The computed overall TOF decreases by a factor
546 of 2.9 going from the vapor phase ($TOF_{\text{overall-vapor}} = 1.95 \times 10^{-4} \text{ s}^{-1}$) to an aqueous phase
547 ($TOF_{\text{overall-water}} = 6.70 \times 10^{-5} \text{ s}^{-1}$). The calculated TOFs along the dominant reaction pathway in
548 different reaction environments are shown in Figure 2. The major product in the aqueous phase is
549 predicted to be phenol ($TOF_{\text{phenol}} = 6.66 \times 10^{-5} \text{ s}^{-1}$), similar to the vapor phase.⁴² However, unlike
550 the vapor phase where catechol was found to be the major side product, in liquid water we found
551 benzene to be the major side product with a two order of magnitude lower production rate than
552 that of phenol ($TOF_{\text{benzene}} = 4.02 \times 10^{-7} \text{ s}^{-1}$) which agrees qualitatively well with experimental
553 studies.^{10,46}

554 As we have reported previously,^{50,75} a fundamental caveat of using a continuum solvation
555 scheme to compute the solvent effects is the uncertainty associated with the cavity radius of
556 transition metal atoms due to a lack of accurate experimental solvation data. To account for the
557 uncertainty of Ru atoms, we performed our aqueous phase calculations at three different cavity
558 radii of Ru atoms: the default cavity radius provided by the TURBOMOLE⁶⁴ program package
559 (2.223 Å), a 10% increased cavity radius (2.445 Å), and a 10% decreased cavity radius (2.0007
560 Å). Our microkinetic model results indicated that the usage of a different cavity radius does not
561 change the dominant reaction mechanism in an aqueous phase. However, we also observed that
562 the overall TOF decreases by 2 orders of magnitude ($TOF_{water}^{COSMO-10} = 1.35 \times 10^{-7} \text{ s}^{-1}$) when we
563 decrease the cavity radius of Ru atoms while with a 10% increase, TOF increases by a factor of
564 1.22 ($TOF_{water}^{COSMO+10} = 8.19 \times 10^{-5} \text{ s}^{-1}$).

565 Hellinger et al.⁴⁴ studied the solvent effect on the HDO of guaiacol over Pt/SiO₂ and Pt/H-
566 MFI 90 catalysts at 450 K and 50 bar hydrogen partial pressure. They surmised that polar solvents
567 lead to a lower conversion of the HDO of guaiacol due to the oxygen containing solvents being
568 strongly adsorbed on the active sites of the catalysts leading to blockage of active sites,⁹³ which
569 partially explains why our model predicted a lower activity of the Ru catalyst in an aqueous phase.
570 Nakagawa et al.³⁶ investigated of HDO of guaiacol over Ru/C catalysts in aqueous phase at a
571 relatively low temperature (433K) and 15 bar H₂ partial pressure. The major products they
572 observed are phenyl ring saturated products such as cyclohexanol, 2-methoxycyclohexanol, and
573 cyclohexane. Addition of MgO to the reaction media increased the yield of cyclohexanol and
574 methanol. Using the same reaction conditions, Ishikawa et al.⁴⁶ studied the HDO of guaiacol over
575 carbon black supported Ru-MnO_x catalyst (Ru-MnO_x/C) and found cyclohexanol and methanol to
576 be the major product. However, in both cases they observed phenol at short reaction times and the

577 selectivity of phenol decreased with guaiacol conversion and cyclohexanol production, which
578 agrees with our calculations of the HDO of guaiacol at low conversion conditions.

579 *II. Less Protic Solvent (1-Butanol, Diethyl ether, and n-Hexane) Effects*

580 Microkinetic models for 1-butanol, diethyl ether, and n-hexane were performed under
581 similar reaction conditions except that we employed a water partial pressure similar to our vapor
582 phase simulations ($P_{H_2O} = 10^{-6}$ bar). Unlike for water, solvent adsorption is not considered in the
583 microkinetic models since at the high reaction temperatures the (vapor phase) adsorption free
584 energy of all solvent molecules is highly endergonic (at 473 K it is 0.31 eV for 1-butanol, 0.51 eV
585 for diethyl ether, and 0.52 eV for n-hexane). As a result, the solvent surface coverage is smaller
586 10^{-2} % under all reaction conditions and does not affect the observed kinetics. Our simulations
587 predict a factor two increase in catalytic activity ($TOF_{1-butanol} = 4.66 \times 10^{-4}$, $TOF_{diethyl\ ether}$
588 $= 4.33 \times 10^{-4}$, $TOF_{n-hexane} = 5.17 \times 10^{-4}$) relative to the vapor phase ($TOF_{1-butanol}$
589 $= 1.95 \times 10^{-4} \text{ s}^{-1}$) for less protic solvents which agrees with the observation of Hellinger et al.⁴⁴
590 that non-polar solvents have a positive effect on the HDO of guaiacol. Except for higher
591 temperatures (>523 K), we found that the presence of a less protic solvent facilitates the phenol
592 production. Chen et al.⁷⁶ reported phenol as an intermediate for HDO of guaiacol over Ru/C at
593 413-533 K and 4 MPa hydrogen partial pressure using ethanol as a solvent, which has a normalized
594 polarity close to that of 1-butanol. Lu et al.⁷⁷ investigated the HDO of guaiacol over Ru/TiO₂,
595 Ru/ZrO₂, and Ru supported on TiO₂-ZrO₂ composite oxides at 473-533K and 2 MPa hydrogen
596 partial pressure using a non-polar solvent, n-dodecane as the reaction medium. They found 2-
597 methoxycyclohexanol, cyclohexanol, and phenol to be the major reaction products at low reaction
598 temperature (473K) which partially confirms our microkinetic model predictions.

599 **4.1.4 Apparent Activation Barrier, Reaction Orders, and Sensitivity Analysis**

600 We calculated the apparent activation barrier (E_a) and reaction orders (n_{gua} , n_{CO} , & n_{H_2})
601 (Table 6), and performed a sensitivity analysis in different reaction environments (Table 7). Going
602 from the vapor to an aqueous phase, the estimated apparent activation barrier for the temperature
603 range of 423 K-573 K increases by 0.03 eV which explains the decrease in TOF in liquid water.
604 In less protic solvents such as 1-butanol, diethyl ether, and n-hexane, we predict very similar
605 apparent activation energies of 1.55 eV, 1.57 eV, and 1.58 eV, respectively. The lower apparent
606 activation energies in less protic solvents can be attributed to the slightly higher number of free
607 sites available compared to that of liquid water (Table 5).

608 Next, we investigated the dependence of the overall TOF on the partial pressures of
609 guaiacol, CO, and H₂, and the results have been summarized in Table 6. An increase in partial
610 pressure of guaiacol increases the reaction rate across all reaction environments with the less protic
611 solvents predicting same reaction order for guaiacol (0.12). Site blocking due to increase in CO
612 partial pressure leads to a negative reaction order for CO in all reaction environments where the
613 aqueous phase shows the most pronounced effect ($n_{CO}^{water} = -0.65$). This phenomenon can be
614 explained by the shift in equilibrium of the decarbonylation step 43 to the reactant (2-carbide-oxy-
615 phenolate to 2-oxyphenyl) in liquid water, resulting in a 99.8% decrease in the TOF for the
616 elementary step while increasing the CO partial pressure from 10⁻⁵ bar 0.10 bar. For less protic
617 solvents, this reaction step does not become more endergonic but exergonic relative to the vapor
618 phase (Table 3), partially explaining why CO poisoning is reduced in these solvents. We also
619 observed an inhibiting effect of low H₂ partial pressure (0.20 – 0.40 bar) in vapor and aqueous
620 phase environments. However, our model indicated that in other less protic solvents, even in the
621 low temperature range, the hydrogen reaction order remains positive. This observation can be
622 attributed to step 46, the CH species removal step from the surface. In vapor and aqueous phases,

623 this reaction step poses a modest (~ 0.60 eV) activation barrier. In the low partial pressure region (
624 $P_{H_2} = 0.20 - 0.40$ bar), the slight increase in hydrogen partial pressure slightly increases the
625 hydrogen coverage but fails to shift the equilibrium of the reaction, thereby reducing the number
626 of free sites available which again leads to an inhibiting effect. Meanwhile, in other protic solvents,
627 due to the low free energy of activation (0.18-0.35 eV), even a slight increase in hydrogen partial
628 pressure is able to move the equilibrium to the right, resulting in an increased number of available
629 free sites that promotes guaiacol adsorption and reaction. Further increase in partial pressure of
630 hydrogen (0.60 - 20.0 bar) shifts the equilibrium to the right, thereby decreasing the poisoning
631 effect of CH and promoting the reaction rate across all reaction environments.

632 To identify the rate controlling steps and surface intermediates, we used Campbell's degree
633 of rate control and degree of thermodynamic rate control⁹⁴⁻⁹⁶ analyses. Results of the sensitivity
634 analyses are summarized in Table 7. We observed that H, CO, and CH have a poisoning effect on
635 the catalyst due to their high surface coverage in vapor and aqueous phase processing conditions
636 such that destabilizing their adsorption increases the overall reaction rate. In less protic reaction
637 environments, the largest degree of rate controlling species was found to be $C_6H_4O_2$ which has a
638 similar poisoning effect on the surface. Due to the high surface coverage of the CH species in
639 vapor and aqueous phases, our model predicts methyl hydrogenation to methane as one of the rate
640 controlling steps in the reaction mechanism. However, in less protic solvents, dehydroxylation of
641 the hydrogen catecholate species ($C_6H_4(OH)O$) to 2-oxyphenyl (C_6H_4O), which serves as a
642 precursor to phenol production, becomes the most rate controlling reaction such that lowering the
643 activation barrier increases the overall reaction rate. Across all reaction environments, our model
644 predicts that CH removal of 2-methyldiene-oxy-phenolate species ($C_6H_4(O)(OCH)$) to catecholate
645 species ($C_6H_4O_2$) has an inhibiting effect while dehydrogenation to 2-carbide-oxy-phenolate

646 intermediate ($C_6H_4(O)(OC)$) facilitates the overall TOF. Owing to a lack of an availability of free
647 sites for catalysis, our model also predicts a moderate degree of rate control for the guaiacol
648 adsorption process.

649

650 **4.2 Hydrogenation of Phenol to Alicyclic Products**

651 **4.2.1 Reaction Network**

652 The hydro-upgrading of phenol to cycloalkanes can occur in a number of different ways.
653 Hydrogen addition steps can happen at the α -C (C_1 pathway), *ortho*- (C_2 pathway), *meta*- (C_3
654 pathway), or *para*- (C_4 pathway) positions of the phenolic ring to produce cyclohexanol and
655 cyclohexanone (Figure 4 and Figure 5). Furthermore, phenol can undergo dehydrogenation to
656 produce a phenoxy species and then go through hydrogenation steps to produce cyclohexanone.
657 Cyclohexanone can then undergo C=O hydrogenation to form cyclohexanol (Keto-enol
658 tautomerization pathway, Figure 6). The naming convention employed in the reaction network
659 schemes is as follows: first hydrogenation of the phenyl ring at C_x position leads to the formation
660 of HCX-1 intermediate species [$X=1, 2, 3, 4$], and subsequent hydrogenated moieties are denoted
661 adding a second integer. Different structures with same number of hydrogenations of phenol are
662 distinguished by adding a letter at the end. For example, HC1-3a (Figure 4) refers to an
663 intermediate species in the C_1 hydrogenation pathway with three hydrogenations of the phenyl
664 ring, the last of which occurs at the C_5 position, while HC1-3b refers to an adsorbed species of the
665 same pathway with same number of hydrogenations, the last of which happening at C_6 position.
666 Finally, cyclohexanol being a species hydrogenated at all six carbons of phenol is denoted as HC-6
667 species.

668 For the keto-enol tautomerization pathway (Figure 7), dehydrogenation of phenol at the hydroxyl
669 group leads to the formation of a phenoxy species (KET-1). Subsequent hydrogenated products
670 along the reaction network are denoted using an integer after 'KET', e.g., KET-5d refers to a
671 phenolate species that has been hydrogenated four times, the last of which occurs at C₆ position.
672 KET-6 (Cyclohexanone) refers to complete hydrogenation of the phenolate species. In total, we
673 investigated 114 elementary steps along the reaction network for phenol hydrogenation to
674 cycloalkanes over a Ru(0001) surface. Table S3 of the supporting information summarizes the free
675 energies of these elementary processes at three different reaction temperatures and Figure S1 and
676 S2 displays the side and top views of the optimized intermediates and transition state structures
677 investigated for this reaction network. In the following sections, we discuss the energetics of these
678 elementary processes in vapor and condensed phases. Unless otherwise stated, the free energies of
679 reaction and free energies of activation are interpreted at a reaction temperature of 473 K.

680

681 4.2.2 Energetics in Vapor Phase

682 In the C₁ pathway, addition of a hydrogen to phenol (step 1) leads to the formation of the
683 HC1-1 species (C₆H₅H_αOH) which is an endergonic process ($\Delta G_{rxn} = 0.41 \text{ eV}$) and requires
684 overcoming a free energy of activation of 1.16 eV. Subsequent hydrogenation to HC1-2a (step 2,
685 second hydrogenation at the *para*- position) or HC1-2b (step 3, second hydrogenation at the *ortho*-
686 position) are both highly endergonic processes with free energies of reaction of 0.85 eV and 0.80
687 eV, respectively (See Table S3). In pathway C₂, hydrogenation of phenol (step 37) results in HC2-1
688 species (C₆H₅H_{ortho}OH) which is a thermodynamically and kinetically challenging process (ΔG_{rxn}
689 = 0.58 eV, $\Delta G^\ddagger = 1.11 \text{ eV}$). HC2-1 can then undergo a second hydrogenation step to produce

690 HC2-2a (step 38) or HC2-2b (step 39) which are again thermodynamically demanding processes
691 ($\Delta G_{rxn}^{38} = 0.62 \text{ eV}$, $\Delta G_{rxn}^{39} = 0.78 \text{ eV}$).

692 Hydrogenation of phenol at the *meta* position (Pathway C₃) leading to the formation of a
693 HC3-1 species (step 52) is a kinetically difficult endergonic process ($\Delta G^\ddagger = 1.05 \text{ eV}$). Second
694 hydrogenations of phenol along this reaction pathway to produce HC3-2a or HC3-2b moieties are
695 also endergonic processes with free energies of reaction of 0.72 eV and 0.74 eV, respectively.
696 Along the C₄ pathway, hydrogenation of phenol (step 77) produces the HC4-1 (C₆H₅H_{para}OH)
697 species which is also an endergonic and kinetically challenging process ($\Delta G_{rxn} = 0.71 \text{ eV}$, ΔG^\ddagger
698 $= 1.15 \text{ eV}$).

699 Finally, in the keto-enol tautomerization pathway (Figure 7), the initial O-H scission of
700 phenol at the hydroxyl group (step 80) was found to be a facile exergonic process (ΔG_{rxn}
701 $= -0.76 \text{ eV}$, $\Delta G^\ddagger = 0.31 \text{ eV}$). Therefore, it is most likely that phenol at first undergoes to
702 dehydrogenation to form a phenolate species before further hydrogenations. Subsequent
703 hydrogenations of the phenolate (KET-1) species to KET-2a (step 81) and KET-2b (step 102) are
704 both thermodynamically challenging processes ($\Delta G_{rxn}^{81} = 0.99 \text{ eV}$, $\Delta G_{rxn}^{102} = 0.94 \text{ eV}$). Due to the
705 enormity of the reaction network, we made use of the Evans-Polanyi principle⁹⁷ at this stage, which
706 points to the favorability of step 102 over step 81 due to its less endergonicity. Thermodynamics
707 of subsequent hydrogenations of the KET-2b species (step 103, 104, 105, and 106) predicts the
708 most thermodynamically favorable pathway to be step 105 to produce the KET-3g species (ΔG_{rxn}
709 $= 0.27 \text{ eV}$, $\Delta G^\ddagger = 0.84 \text{ eV}$). Next, KET-3g is hydrogenated to KET-4d (step 109) which is an
710 endergonic process with challenging kinetics ($\Delta G_{rxn} = 0.42 \text{ eV}$, $\Delta G^\ddagger = 1.06 \text{ eV}$). KET-4d
711 intermediate, which is the same as KET-4b, is subsequently hydrogenated to KET-5c (step 92) or
712 KET-5d (step 93), of which the former is thermodynamically more favorable ($\Delta G_{rxn}^{92} = 0.17 \text{ eV}$, Δ

713 $G_{rxn}^{93} = 0.82 \text{ eV}$) with a free energy of activation of 1.07 eV. KET-5c then undergoes
 714 hydrogenation (step 96) to produce KET-6 (Cyclohexanone) with a moderately endergonic
 715 reaction free energy ($\Delta G_{rxn} = 0.32 \text{ eV}$) and a high free energy of activation ($\Delta G^\ddagger = 1.21 \text{ eV}$).
 716 KET-6 finally undergoes hydrogenation at the hydroxyl group to form KET-7a (step 98) and
 717 subsequently hydrogenated (step 100) to produce HC-6 (Cyclohexanol). Although kinetically very
 718 demanding, on the basis of these energetics calculations alone, the likely pathway to produce
 719 cyclohexanol from phenol proceeds through,

720 $Phenol \rightarrow KET-1 \rightarrow KET-2b \rightarrow KET-3g \rightarrow KET-4b \rightarrow KET-5c \rightarrow KET-6 \rightarrow KET-7a \rightarrow HC-6$. This

721 probable pathway is highlighted in Figure 6. Next, we look into the condensed phase effects on
 722 this more likely path to understand if the presence of a solvent causes differences.

723 4.2.3 Energetics in Liquid Phase

724 Table 8 summarizes the thermodynamics and kinetics of the important elementary surface
 725 processes for hydrogenation of phenol in various reaction environments. Presence of a solvent
 726 barely affects the thermodynamics or the kinetics of phenolate (KET-1) production from phenol
 727 (step 80) or the subsequent hydrogenation steps to form the KET-2b species (step 102) and KET-
 728 3g species (step 105). However, liquid water reduces the free energy of activation of the next
 729 hydrogenation step to produce KET-4d/b species (step 109) by 0.13 eV where the non-polar aprotic
 730 n-hexane demonstrates a less dramatic effect. Introduction of a liquid phase environment also
 731 facilitates the subsequent hydrogenation of KET-4b to KET-5c (step 92), with water displaying
 732 the largest facilitating effect ($\Delta(\Delta G_{water}^\ddagger) = -0.17 \text{ eV}$). KET-5c then undergoes hydrogenation to
 733 produce the KET-6 species (step 96) where condensed phases have a nominal effect on the
 734 thermodynamics of the reaction. However, the reaction becomes more facile in the liquid phase,
 735 with liquid water reducing the free energy of activation by 0.17 eV. The thermodynamics and

736 kinetics of the final two subsequent hydrogenation steps (step 98 & 100) are minimally affected
737 by the presence of a condensed phase. Overall, addition of a liquid phase reaction medium
738 facilitates the likely pathway proposed in the previous section with liquid water exhibiting the
739 largest facilitating effect which compares favorably with the experimental observation of Zhong
740 et al.⁹² However, the kinetics of some of these elementary processes (Table 8) still remains very
741 demanding.

742

743 **5. Conclusions**

744 The solvent influence on the hydrodeoxygenation of guaiacol over a Ru(0001) model
745 surface has been investigated by means of periodic DFT calculations, non-periodic implicit
746 solvation calculations with iSMS scheme, and microkinetic modeling. In the first step, we
747 examined the formation of unsaturated aromatic products such as phenol, anisole, catechol etc.
748 from guaiacol. We developed mean-field microkinetic reactor models at different temperatures
749 and experimental reaction conditions.^{36,46} Under all reaction environments and reaction conditions,
750 we found the same dominating HDO mechanism with the most favored pathway following the
751 initial dehydrogenation at the hydroxyl group of guaiacol, followed by complete dehydrogenation
752 of the methoxy group and subsequent decarbonylation, which then undergoes two subsequent
753 hydrogenations to produce phenol. Less protic solvents such as 1-butanol, diethyl ether, and n-
754 hexane demonstrate a higher HDO rate compared to that of vapor and aqueous phases which is
755 qualitatively in good agreement with experimental results.⁴⁴ After verifying the presence of
756 phenol, which is often referred to as a ‘short-lived intermediate’, we investigated the production
757 of cycloalkanes through phenol hydrogenation in vapor and condensed phases. We observed that
758 dehydrogenation of phenol to a phenolate species (keto-enol tautomerization pathway) is the most

759 likely pathway to produce cyclohexanol and cyclohexanone from phenol. Based on the vapor
760 phase first-principles calculations, we proposed a plausible pathway for cycloalkane formation.
761 Next, we investigated the solvent effects on this probable reaction pathway and demonstrated a
762 facilitating effect of an aqueous phase along the proposed reaction mechanism which is again in
763 line with experimental observations.⁹⁸ Therefore, our study addresses a crucial issue, how the
764 presence of a condensed phase affects the hydrogenation of aromatic rings over Ru catalysts. We
765 note here that the proposed pathway still remains kinetically very challenging and it is possible
766 that the cyclohexanone and cyclohexanol production follows a different reaction route along the
767 keto-enol tautomerization pathway. Prior investigations have also shown that the support can play
768 a major role in the hydrogenation of phenol which might also facilitate the kinetics of the reactions
769 along the hypothesized reaction mechanism.⁸⁹ However, a full computational investigation of the
770 phenol hydrogenation is out of the scope of the present study and we encourage further
771 computational investigations on phenol hydrogenation for the production of cycloalkanes.
772 Nevertheless, we can conclude that solvents with high degree of polarity are favorable for
773 hydrogenation of the phenyl ring over Ru catalysts while non-polar solvents tend to facilitate the
774 demethoxylation of guaiacol species.

775

776 **Associated Content**

777 Supporting Information

778 The Supporting Information is available free of charge on the ACS Publications website at DOI:

779 XXX

780 Lateral interaction parameters employed in the microkinetic model, Kamlet and Taft
781 solvatochromic parameters, free energies of elementary reaction at different temperatures,
782 geometries of adsorbed intermediates and transition states.

783 **Notes**

784 The authors declare no competing financial interests.

785 **Acknowledgements**

786 We gratefully acknowledge the financial support of United States Department of Energy, Office
787 of Basic Energy Sciences (DE-SC0007167). Computing resources provided by the National
788 Energy Research Scientific Computing Center (NERSC), Texas Advanced Computing Center
789 (TACC), and Pacific Northwest National Laboratory (PNNL) are gratefully acknowledged.

790

791 **References**

- 792 1. Li, Z.; Han, C.; Gu, T. Economics of biomass gasification: A review of the current status.
793 *Energy Sources, Part B: Economics, Planning, and Policy* **2018**, *13*, 137-140.
- 794 2. Popp, J.; Lakner, Z.; Harangi-Rakos, M.; Fari, M. The effect of bioenergy expansion: Food,
795 energy, and environment. *Renew Sust Energy Rev* **2014**, *32*, 559-578.
- 796 3. Carriquiry, M. A.; Du, X. D.; Timilsina, G. R. Second generation biofuels: Economics and
797 policies. *Energy Policy* **2011**, *39*, 4222-4234.
- 798 4. Chheda, J. N.; Huber, G. W.; Dumesic, J. A. Liquid-phase catalytic processing of biomass-
799 derived oxygenated hydrocarbons to fuels and chemicals. *Angewandte Chemie-International*
800 *Edition* **2007**, *46*, 7164-7183.
- 801 5. Alonso, D. M.; Bond, J. Q.; Dumesic, J. A. Catalytic conversion of biomass to biofuels. *Green*
802 *Chem* **2010**, *12*, 1493-1513.
- 803 6. Serrano-Ruiz, J. C.; Dumesic, J. A. Catalytic routes for the conversion of biomass into liquid
804 hydrocarbon transportation fuels. *Energy Environ Sci* **2011**, *4*, 83-99.
- 805 7. Xiu, S. N.; Shahbazi, A. Bio-oil production and upgrading research: A review. *Renew Sust*
806 *Energy Rev* **2012**, *16*, 4406-4414.
- 807 8. Furimsky, E. Catalytic hydrodeoxygenation. *Appl Catal a-Gen* **2000**, *199*, 147-190.
- 808 9. Honkela, M. L.; Viljava, T.-R.; Gutierrez, A.; Krause, A. O. I. In *Thermochemical Conversion*
809 *of Biomass to Liquid Fuels and Chemicals*, The Royal Society of Chemistry, **2010**, pp. 288-306
- 810 10. Elliott, D. C.; Hart, T. R. Catalytic Hydroprocessing of Chemical Models for Bio-oil. *Energy*
811 *Fuel* **2009**, *23*, 631-637.
- 812 11. Popov, A.; Kondratieva, E.; Mariey, L.; Goupil, J. M.; El Fallah, J.; Gilson, J. P.; Travert, A.;
813 Mauge, F. Bio-oil hydrodeoxygenation: Adsorption of phenolic compounds on sulfided (Co)Mo
814 catalysts. *J Catal* **2013**, *297*, 176-186.
- 815 12. Zhang, S. P.; Yan, Y. J.; Li, T. C.; Ren, Z. W. Upgrading of liquid fuel from the pyrolysis of
816 biomass. *Bioresource Technol* **2005**, *96*, 545-550.
- 817 13. Wildschut, J.; Mahfud, F. H.; Venderbosch, R. H.; Heeres, H. J. Hydrotreatment of Fast
818 Pyrolysis Oil Using Heterogeneous Noble-Metal Catalysts. *Ind Eng Chem Res* **2009**, *48*, 10324-
819 10334.
- 820 14. Viljava, T. R.; Komulainen, S.; Selvam, T.; Krause, A. O. I. Stability of CoMo/Al₂O₃ catalysts:
821 Effect of HDO cycles on HDS. *Stud Surf Sci Catal* **1999**, *127*, 145-152.
- 822 15. Viljava, T. R.; Komulainen, R. S.; Krause, A. O. I. Effect of H₂S on the stability of
823 CoMo/Al₂O₃ catalysts during hydrodeoxygenation. *Catal Today* **2000**, *60*, 83-92.
- 824 16. Gutierrez, A.; Kaila, R. K.; Honkela, M. L.; Slioor, R.; Krause, A. O. I. Hydrodeoxygenation
825 of guaiacol on noble metal catalysts. *Catal Today* **2009**, *147*, 239-246.
- 826 17. Furimsky, E.; Massoth, F. Deactivation of hydroprocessing catalysts. *Catalysis Today* **1999**,
827 *52*, 381-495.
- 828 18. Laurent, E.; Centeno, A.; Delmon, B. Coke Formation during the Hydrotreating of Biomass
829 Pyrolysis Oils - Influence of Guaiacol Type Compounds. *Catalyst Deactivation 1994* **1994**, *88*, 573-
830 578.
- 831 19. Laurent, E.; Delmon, B. Influence of Water in the Deactivation of a Sulfided Nimo Gamma-
832 Al₂O₃ Catalyst during Hydrodeoxygenation. *J Catal* **1994**, *146*, 281-291.

- 833 20. Lin, Y. C.; Li, C. L.; Wan, H. P.; Lee, H. T.; Liu, C. F. Catalytic Hydrodeoxygenation of Guaiacol
834 on Rh-Based and Sulfided CoMo and NiMo Catalysts. *Energ Fuel* **2011**, *25*, 890-896.
- 835 21. Mortensen, P. M.; Grunwaldt, J. D.; Jensen, P. A.; Knudsen, K. G.; Jensen, A. D. A review
836 of catalytic upgrading of bio-oil to engine fuels. *Appl Catal a-Gen* **2011**, *407*, 1-19.
- 837 22. Holladay, J. E.; White, J. F.; Bozell, J. J.; Johnson, D. In *Top Value Added Chemicals from*
838 *Biomass - Volume II, Results of Screening for Potential Candidates from Biorefinery Lignin*, Pacific
839 Northwest National Lab., Richland, WA: 2007; pp 42-44.
- 840 23. Zakzeski, J.; Jongorius, A. L.; Bruijninx, P. C. A.; Weckhuysen, B. M. Catalytic Lignin
841 Valorization Process for the Production of Aromatic Chemicals and Hydrogen. *Chemsuschem*
842 **2012**, *5*, 1602-1609.
- 843 24. Gonzalez-Borja, M. A.; Resasco, D. E. Anisole and Guaiacol Hydrodeoxygenation over
844 Monolithic Pt-Sn Catalysts. *Energ Fuel* **2011**, *25*, 4155-4162.
- 845 25. Nimmanwudipong, T.; Runnebaum, R. C.; Block, D. E.; Gates, B. C. Catalytic Conversion of
846 Guaiacol Catalyzed by Platinum Supported on Alumina: Reaction Network Including
847 Hydrodeoxygenation Reactions. *Energ Fuel* **2011**, *25*, 3417-3427.
- 848 26. Lee, C. R.; Yoon, J. S.; Suh, Y. W.; Choi, J. W.; Ha, J. M.; Suh, D. J.; Park, Y. K. Catalytic roles
849 of metals and supports on hydrodeoxygenation of lignin monomer guaiacol. *Catal Commun* **2012**,
850 *17*, 54-58.
- 851 27. Nimmanwudipong, T.; Aydin, C.; Lu, J.; Runnebaum, R. C.; Brodwater, K. C.; Browning, N.
852 D.; Block, D. E.; Gates, B. C. Selective Hydrodeoxygenation of Guaiacol Catalyzed by Platinum
853 Supported on Magnesium Oxide. *Catal Lett* **2012**, *142*, 1190-1196.
- 854 28. Sun, J. M.; Karim, A. M.; Zhang, H.; Kovarik, L.; Li, X. H. S.; Hensley, A. J.; McEwen, J. S.;
855 Wang, Y. Carbon-supported bimetallic Pd-Fe catalysts for vapor-phase hydrodeoxygenation of
856 guaiacol. *J Catal* **2013**, *306*, 47-57.
- 857 29. He, Z.; Wang, X. Q. Highly selective catalytic hydrodeoxygenation of guaiacol to
858 cyclohexane over Pt/TiO₂ and NiMo/Al₂O₃ catalysts. *Front Chem Sci Eng* **2014**, *8*, 369-377.
- 859 30. Gao, D.; Schweitzer, C.; Hwang, H. T.; Varma, A. Conversion of Guaiacol on Noble Metal
860 Catalysts: Reaction Performance and Deactivation Studies. *Ind Eng Chem Res* **2014**, *53*, 18658-
861 18667.
- 862 31. Gao, D. N.; Xiao, Y.; Varma, A. Guaiacol Hydrodeoxygenation over Platinum Catalyst:
863 Reaction Pathways and Kinetics. *Ind Eng Chem Res* **2015**, *54*, 10638-10644.
- 864 32. Lin, Y.-C.; Li, C.-L.; Wan, H.-P.; Lee, H.-T.; Liu, C.-F. Catalytic Hydrodeoxygenation of
865 Guaiacol on Rh-Based and Sulfided CoMo and NiMo Catalysts. *Energy & Fuels* **2011**, *25*, 890-896.
- 866 33. Chang, J.; Danuthai, T.; Dewiyanti, S.; Wang, C.; Borgna, A. Hydrodeoxygenation of
867 Guaiacol over Carbon-Supported Metal Catalysts. *Chemcatchem* **2013**, *5*, 3041-3049.
- 868 34. Hong, Y. K.; Lee, D. W.; Eom, H. J.; Lee, K. Y. The catalytic activity of Pd/WO_x/gamma-
869 Al₂O₃ for hydrodeoxygenation of guaiacol. *Appl Catal B-Environ* **2014**, *150*, 438-445.
- 870 35. Boonyasuwat, S.; Omotoso, T.; Resasco, D. E.; Crossley, S. P. Conversion of Guaiacol over
871 Supported Ru Catalysts. *Catal Lett* **2013**, *143*, 783-791.
- 872 36. Nakagawa, Y.; Ishikawa, M.; Tamura, M.; Tomishige, K. Selective production of
873 cyclohexanol and methanol from guaiacol over Ru catalyst combined with MgO. *Green Chem*
874 **2014**, *16*, 2197-2203.

- 875 37. Olcese, R. N.; Bettahar, M.; Petitjean, D.; Malaman, B.; Giovanella, F.; Dufour, A. Gas-
876 phase hydrodeoxygenation of guaiacol over Fe/SiO₂ catalyst. *Applied Catalysis B: Environmental*
877 **2012**, *115-116*, 63-73.
- 878 38. Bykova, M. V.; Ermakov, D. Y.; Kaichev, V. V.; Bulavchenko, O. A.; Saraev, A. A.; Lebedev,
879 M. Y.; Yakovlev, V. A. Ni-based sol-gel catalysts as promising systems for crude bio-oil upgrading:
880 Guaiacol hydrodeoxygenation study. *Appl Catal B-Environ* **2012**, *113*, 296-307.
- 881 39. Honkela, M. L.; Viljava, T. R.; Gutierrez, A.; Krause, A. O. I. Hydrotreating for Bio-Oil
882 Upgrading. *Rsc Energy Environ S* **2010**, 288-306.
- 883 40. Schimming, S. M.; LaMont, O. D.; Konig, M.; Rogers, A. K.; D'Amico, A. D.; Yung, M. M.;
884 Sievers, C. Hydrodeoxygenation of Guaiacol over Ceria-Zirconia Catalysts. *Chemsuschem* **2015**, *8*,
885 2073-2083.
- 886 41. Wildschut, J.; Mahfud, F.; Venderbosch, R.; Heeres, H. Hydrotreatment of Fast Pyrolysis
887 Oil Using Heterogeneous Noble-Metal Catalysts. *Industrial & Engineering Chemistry Research*
888 **2009**, *48*, 10324-10334.
- 889 42. Lu, J. M.; Heyden, A. Theoretical investigation of the reaction mechanism of the
890 hydrodeoxygenation of guaiacol over a Ru(0001) model surface. *J Catal* **2015**, *321*, 39-50.
- 891 43. Narayan, S.; Muldoon, J.; Finn, M.; Fokin, V.; Kolb, H.; Sharpless, K. "On water": Unique
892 reactivity of organic compounds in aqueous suspension. *Angewandte Chemie-International*
893 *Edition* **2005**, *44*, 3275-3279.
- 894 44. Hellinger, M.; de Carvalho, H. W. P.; Baier, S.; Gharnati, L.; Grunwaldt, J. D. Solvent
895 Influence on the Hydrodeoxygenation of Guaiacol over Pt/SiO₂ and Pt/H-MFI90 Catalysts. *Chem-*
896 *Ing-Tech* **2015**, *87*, 1771-1780.
- 897 45. Hellinger, M.; Baier, S.; Mortensen, P. M.; Kleist, W.; Jensen, A. D.; Grunwaldt, J. D.
898 Continuous Catalytic Hydrodeoxygenation of Guaiacol over Pt/SiO₂ and Pt/H-MFI-90. *Catalysts*
899 **2015**, *5*, 1152-1166.
- 900 46. Ishikawa, M.; Tamura, M.; Nakagawa, Y.; Tomishige, K. Demethoxylation of guaiacol and
901 methoxybenzenes over carbon-supported Ru-Mn catalyst. *Appl Catal B-Environ* **2016**, *182*, 193-
902 203.
- 903 47. Reichardt, C.; Welton, T. In *Solvents and Solvent Effects in Organic Chemistry*, Reichardt,
904 C.; Welton, T., Eds.; Wiley-VCH: Weinheim, Germany, **2011**; pp 425-508.
- 905 48. Faheem, M.; Suthirakun, S.; Heyden, A. New Implicit Solvation Scheme for Solid Surfaces.
906 *J Phys Chem C* **2012**, *116*, 22458-22462.
- 907 49. Yoon, J. S.; Choi, J. W.; Suh, D. J.; Lee, K.; Lee, H.; Ha, J. M. Water-Assisted Selective
908 Hydrodeoxygenation of Lignin-Derived Guaiacol to Monooxygenates. *Chemcatchem* **2015**, *7*,
909 2669-2674.
- 910 50. Saleheen, M.; Heyden, A. Liquid-Phase Modeling in Heterogeneous Catalysis. *Acs Catal*
911 **2018**, *8*, 2188-2194.
- 912 51. Behtash, S.; Lu, J. M.; Faheem, M.; Heyden, A. Solvent effects on the hydrodeoxygenation
913 of propanoic acid over Pd(111) model surfaces (vol 16, pg 605, 2014). *Green Chem* **2014**, *16*,
914 4427-4428.
- 915 52. Behtash, S.; Lu, J. M.; Walker, E.; Mamun, O.; Heyden, A. Solvent effects in the liquid phase
916 hydrodeoxygenation of methyl propionate over a Pd(111) catalyst model. *J Catal* **2016**, *333*, 171-
917 183.

- 918 53. Behtash, S.; Lu, J. M.; Mamun, O.; Williams, C. T.; Monnier, J. R.; Heyden, A. Solvation
919 Effects in the Hydrodeoxygenation of Propanoic Acid over a Model Pd(211) Catalyst. *J Phys Chem*
920 *C* **2016**, *120*, 2724-2736.
- 921 54. Mamun, O.; Saleheen, M.; Bond, J. Q.; Heyden, A. Importance of Angelica Lactone
922 Formation in the Hydrodeoxygenation of Levulinic Acid to gamma-Valerolactone over a Ru(0001)
923 Model Surface. *J Phys Chem C* **2017**, *121*, 18746-18761.
- 924 55. Klamt, A. Conductor-Like Screening Model for Real Solvents - a New Approach to the
925 Quantitative Calculation of Solvation Phenomena. *J Phys Chem-Us* **1995**, *99*, 2224-2235.
- 926 56. Klamt, A. In *COSMO-RS: From Quantum Chemistry to Fluid Phase Thermodynamics and*
927 *Drug Design*, 1st ed.; Elsevier Science Ltd.: Amsterdam, Netherlands, 2005.
- 928 57. Wellendorff, J.; Lundgaard, K. T.; Møgelhøj, A.; Petzold, V.; Landis, D. D.; Nørskov, J. K.;
929 Bligaard, T.; Jacobsen, K. W. Density functionals for surface science: Exchange-correlation model
930 development with Bayesian error estimation. *Phys Rev B* **2012**, *85*, 235149.
- 931 58. Wellendorff, J.; Silbaugh, T. L.; Garcia-Pintos, D.; Norskov, J. K.; Bligaard, T.; Studt, F.;
932 Campbell, C. T. A benchmark database for adsorption bond energies to transition metal surfaces
933 and comparison to selected DFT functionals. *Surf Sci* **2015**, *640*, 36-44.
- 934 59. Liu, W.; Tkatchenko, A.; Scheffler, M. Modeling Adsorption and Reactions of Organic
935 Molecules at Metal Surfaces. *Accounts of Chemical Research* **2014**, *47*, 3369-3377.
- 936 60. Studt, F.; Abild-Pedersen, F.; Varley, J. B.; Norskov, J. K. CO and CO₂ Hydrogenation to
937 Methanol Calculated Using the BEEF-vdW Functional. *Catal Lett* **2013**, *143*, 71-73.
- 938 61. Studt, F.; Behrens, M.; Kunkes, E. L.; Thomas, N.; Zander, S.; Tarasov, A.; Schumann, J.;
939 Frei, E.; Varley, J. B.; Abild-Pedersen, F.; Norskov, J. K.; Schlogl, R. The Mechanism of CO and CO₂
940 Hydrogenation to Methanol over Cu-Based Catalysts. *Chemcatchem* **2015**, *7*, 1105-1111.
- 941 62. Perdew, J. P.; Burke, K.; Ernzerhof, M. Generalized gradient approximation made simple.
942 *Phys Rev Lett* **1996**, *77*, 3865-3868.
- 943 63. Grimme, S.; Antony, J.; Ehrlich, S.; Krieg, H. A consistent and accurate ab initio
944 parametrization of density functional dispersion correction (DFT-D) for the 94 elements H-Pu. *J*
945 *Chem Phys* **2010**, *132*.
- 946 64. Ahlrichs, R.; Bar, M.; Haser, M.; Horn, H.; Kolmel, C. Electronic-Structure Calculations on
947 Workstation Computers - the Program System Turbomole. *Chem Phys Lett* **1989**, *162*, 165-169.
- 948 65. Von Arnim, M.; Ahlrichs, R. Performance of parallel TURBOMOLE for density functional
949 calculations. *J Comput Chem* **1998**, *19*, 1746-1757.
- 950 66. Weigend, F.; Ahlrichs, R. Balanced basis sets of split valence, triple zeta valence and
951 quadruple zeta valence quality for H to Rn: Design and assessment of accuracy. *Phys Chem Chem*
952 *Phys* **2005**, *7*, 3297-3305.
- 953 67. Russo, T. V.; Martin, R. L.; Hay, P. J. Effective Core Potentials for Dft Calculations. *J Phys*
954 *Chem-Us* **1995**, *99*, 17085-17087.
- 955 68. Becke, A. D. Density-Functional Exchange-Energy Approximation with Correct
956 Asymptotic-Behavior. *Phys Rev A* **1988**, *38*, 3098-3100.
- 957 69. Perdew, J. P. Density-Functional Approximation for the Correlation-Energy of the
958 Inhomogeneous Electron-Gas. *Phys Rev B* **1986**, *33*, 8822-8824.
- 959 70. Eichkorn, K.; Treutler, O.; Ohm, H.; Haser, M.; Ahlrichs, R. Auxiliary Basis-Sets to
960 Approximate Coulomb Potentials. *Chem Phys Lett* **1995**, *240*, 283-289.

- 961 71. Weigend, F. Accurate Coulomb-fitting basis sets for H to Rn. *Phys Chem Chem Phys* **2006**,
962 8, 1057-1065.
- 963 72. Eichkorn, K.; Weigend, F.; Treutler, O.; Ahlrichs, R. Auxiliary basis sets for main row atoms
964 and transition metals and their use to approximate Coulomb potentials. *Theor Chem Acc* **1997**,
965 97, 119-124.
- 966 73. Klamt, A.; Schuurmann, G. Cosmo - a New Approach to Dielectric Screening in Solvents
967 with Explicit Expressions for the Screening Energy and Its Gradient. *J Chem Soc, Perkin Trans 2*
968 **1993**, 799-805.
- 969 74. Schafer, A.; Klamt, A.; Sattel, D.; Lohrenz, J. C. W.; Eckert, F. COSMO Implementation in
970 TURBOMOLE: Extension of an efficient quantum chemical code towards liquid systems. *Phys*
971 *Chem Chem Phys* **2000**, 2, 2187-2193.
- 972 75. Faheem, M.; Saleheen, M.; Lu, J. M.; Heyden, A. Ethylene glycol reforming on Pt(111):
973 first-principles microkinetic modeling in vapor and aqueous phases. *Catal Sci Technol* **2016**, 6,
974 8242-8256. *A new transition state for primary C-H cleavage of ethylene glycol was later found
975 which has 0.10 eV lower energy than reported herein.
- 976 76. Chen, W.; Luo, Z. Y.; Yu, C. J.; Yang, Y.; Li, G. X.; Zhang, J. X. Catalytic conversion of guaiacol
977 in ethanol for bio-oil upgrading to stable oxygenated organics. *Fuel Process Technol* **2014**, 126,
978 420-428.
- 979 77. Lu, M. H.; Du, H.; Wei, B.; Zhu, J.; Li, M. S.; Shan, Y. H.; Shen, J. Y.; Song, C. S.
980 Hydrodeoxygenation of Guaiacol on Ru Catalysts: Influence of TiO₂-ZrO₂ Composite Oxide
981 Supports. *Ind Eng Chem Res* **2017**, 56, 12070-12079.
- 982 78. Zhao, C.; He, J. Y.; Lemonidou, A. A.; Li, X. B.; Lercher, J. A. Aqueous-phase
983 hydrodeoxygenation of bio-derived phenols to cycloalkanes. *J Catal* **2011**, 280, 8-16.
- 984 79. Kamlet, M. J.; Taft, R. W. Solvatochromic Comparison Method .1. Beta-Scale of Solvent
985 Hydrogen-Bond Acceptor (Hba) Basicities. *J Am Chem Soc* **1976**, 98, 377-383.
- 986 80. Yokoyama, T.; Taft, R. W.; Kamlet, M. J. Solvatochromic Comparison Method .3.
987 Hydrogen-Bonding by Some 2-Nitroaniline Derivatives. *J Am Chem Soc* **1976**, 98, 3233-3237.
- 988 81. Taft, R. W.; Kamlet, M. J. Solvatochromic Comparison Method .2. Alpha-Scale of Solvent
989 Hydrogen-Bond Donor (Hbd) Acidities. *J Am Chem Soc* **1976**, 98, 2886-2894.
- 990 82. Mcquarrie, D. A. In *Statistical Mechanics*, 1st ed.; Harper and Row, New York, **1976**, pp.
991 21-141.
- 992 83. Pechukas, P. Transition-State Theory. *Annu Rev Phys Chem* **1981**, 32, 159-177.
- 993 84. Kandoi, S.; Greeley, J.; Sanchez-Castillo, M. A.; Evans, S. T.; Gokhale, A. A.; Dumesic, J. A.;
994 Mavrikakis, M. Prediction of experimental methanol decomposition rates on platinum from first
995 principles. *Top Catal* **2006**, 37, 17-28.
- 996 85. Mamun, O.; Walker, E.; Faheem, M.; Bond, J. Q.; Heyden, A. Theoretical Investigation of
997 the Hydrodeoxygenation of Levulinic Acid to gamma-Valerolactone over Ru(0001). *ACS Catal*
998 **2017**, 7, 215-228.
- 999 86. Getman, R. B.; Schneider, W. F. DFT-based characterization of the multiple adsorption
1000 modes of nitrogen oxides on Pt(111). *J Phys Chem C* **2007**, 111, 389-397.
- 1001 87. Xu, Y.; Getman, R. B.; Shelton, W.; Schneider, W. F. A first-principles investigation of the
1002 effect of Pt cluster size on CO and NO oxidation intermediates and energetics. *Phys Chem Chem*
1003 *Phys* **2008**, 39, 6009-6018.

- 1004 88. Grabow, L. C.; Hvolbaek, B.; Norskov, J. K. Understanding Trends in Catalytic Activity: The
1005 Effect of Adsorbate-Adsorbate Interactions for CO Oxidation Over Transition Metals. *Top Catal*
1006 **2010**, *53*, 298-310.
- 1007 89. Wang, Y.; Yao, J.; Li, H. R.; Su, D. S.; Antonietti, M. Highly Selective Hydrogenation of
1008 Phenol and Derivatives over a Pd@Carbon Nitride Catalyst in Aqueous Media. *J Am Chem Soc*
1009 **2011**, *133*, 2362-2365.
- 1010 90. He, J.; Lu, X. H.; Shen, Y.; Jing, R.; Nie, R. F.; Zhou, D.; Xia, Q. H. Highly selective
1011 hydrogenation of phenol to cyclohexanol over nano silica supported Ni catalysts in aqueous
1012 medium. *Mol Catal* **2017**, *440*, 87-95.
- 1013 91. Giraldo, L.; Bastidas-Barranco, M.; Moreno-Pirajan, J. C. Vapour Phase Hydrogenation of
1014 Phenol over Rhodium on SBA-15 and SBA-16. *Molecules* **2014**, *19*, 20594-20612.
- 1015 92. Liu, H. Z.; Jiang, T.; Han, B. X.; Liang, S. G.; Zhou, Y. X. Selective Phenol Hydrogenation to
1016 Cyclohexanone Over a Dual Supported Pd-Lewis Acid Catalyst. *Science* **2009**, *326*, 1250-1252.
- 1017 93. He, J. Y.; Zhao, C.; Lercher, J. A. Impact of solvent for individual steps of phenol
1018 hydrodeoxygenation with Pd/C and HZSM-5 as catalysts. *J Catal* **2014**, *309*, 362-375.
- 1019 94. Campbell, C. T. Micro- and macro-kinetics: their relationship in heterogeneous catalysis.
1020 *Top Catal* **1994**, *1*, 353-366.
- 1021 95. Campbell, C. T. Finding the rate-determining step in a mechanism - Comparing DeDonder
1022 relations with the "degree of rate control". *J Catal* **2001**, *204*, 520-524.
- 1023 96. Stegelmann, C.; Andreasen, A.; Campbell, C. T. Degree of Rate Control: How Much the
1024 Energies of Intermediates and Transition States Control Rates. *J Am Chem Soc* **2009**, *131*, 8077-
1025 8082.
- 1026 97. Evans, M. G.; Polanyi, M. Further considerations on the thermodynamics of chemical
1027 equilibria and reaction rates. *T Faraday Soc* **1936**, *32*, 1333-1359.
- 1028 98. Zhong, J. W.; Chen, J. Z.; Chen, L. M. Selective hydrogenation of phenol and related
1029 derivatives. *Catal Sci Technol* **2014**, *4*, 3555-3569.
- 1030 99. Kresse, G.; Hafner, J. *Ab initio* molecular dynamics for liquid metals. *Phys. Rev. B: Condens.*
1031 *Matter Mater. Phys.* **1993**, *47*, 558-561.
- 1032 100. Tshepelevitsh, S.; Oss, M.; Pung, A.; Leito, I. Evaluating the COSMO-RS Method for
1033 Modeling Hydrogen Bonding in Solution. *ChemPhysChem* **2013**, *14*, 1909-1919.
- 1034 101. Saleheen, M.; Zare, M.; Faheem, M.; Heyden, A. Computational Investigation of Aqueous
1035 Phase Effects on the Dehydrogenation and Dehydroxylation of Polyols over Pt(111) *J Phys Chem*
1036 **C 2019** *123* (31), 19052-19065

1037
1038
1039
1040

1041

1042 Table 1. Solvent effects on the adsorption strength of various surface intermediates in the HDO
 1043 of guaiacol over a Ru(0001) model surface at 473 K.

1044

Surface Intermediates	Water $\Delta(\Delta G)$ (eV)	1-Butanol $\Delta(\Delta G)$ (eV)	Diethyl ether $\Delta(\Delta G)$ (eV)	n-Hexane $\Delta(\Delta G)$ (eV)
C ₆ H ₄ (OH)(OCH ₃)	-0.22	-0.47	-0.43	-0.33
C ₆ H ₄ H _β (OH)(OCH ₃)	-0.18	-0.36	-0.34	-0.25
C ₆ H ₄ H _α (OH)(OCH ₃)	-0.19	-0.53	-0.50	-0.39
C ₆ H ₄ OCH ₃	-0.07	-0.35	-0.33	-0.24
C ₆ H ₄ OH	-0.20	-0.33	-0.31	-0.22
C ₆ H ₄ (OH)(OCH ₂)	-0.15	-0.43	-0.40	-0.30
C ₆ H ₄ (OH)(O)	-0.22	-0.26	-0.23	-0.15
C ₆ H ₄ (O)(OCH ₃)	-0.16	-0.35	-0.31	-0.22
C ₆ H ₄ H _β (OH)(OCH ₂)	-0.37	-0.38	-0.35	-0.26
C ₆ H ₅ OCH ₃	-0.25	-0.41	-0.38	-0.29
C ₆ H ₄ (OH)(OCH)	-0.17	-0.44	-0.41	-0.30
C ₆ H ₄ (OH) ₂	-0.22	-0.39	-0.36	-0.25
C ₆ H ₄ O	-0.05	-0.33	-0.31	-0.22
C ₆ H ₄ (O)(OCH ₂)	-0.14	-0.29	-0.25	-0.17
C ₆ H ₄ H _β (OH)(O)	-0.19	-0.33	-0.29	-0.20
C ₆ H ₅ OCH ₂	-0.17	-0.32	-0.28	-0.19
C ₆ H ₅ O	-0.13	-0.32	-0.29	-0.20
C ₆ H ₅ OH	-0.20	-0.38	-0.35	-0.26
C ₆ H ₅ (OH) ₂	-0.14	-0.28	-0.25	-0.18
C ₆ H ₄ O ₂	-0.26	-0.34	-0.31	-0.23
C ₆ H ₅	-0.14	-0.31	-0.29	-0.21
C ₆ H ₆ OH	-0.22	-0.28	-0.25	-0.17
C ₆ H ₆	-0.11	-0.26	-0.24	-0.17
C ₆ H ₄ H _α (O)(OH)	-0.19	-0.27	-0.24	-0.17
C ₆ H ₄ (O)(OCH)	-0.18	-0.34	-0.32	-0.24
C ₆ H ₄ (O)(OC)	-0.27	-0.32	-0.29	-0.20
H	0.04	0.01	0.01	0.01
OH	0.04	-0.02	-0.02	0.01
H ₂ O	0.01	-0.10	-0.09	-0.05
CH	-0.05	-0.02	-0.01	0.01
CH ₂	0.02	-0.02	-0.01	0.00
CH ₃	0.11	-0.01	-0.01	0.00
CH ₄	0.04	-0.03	-0.03	-0.03
CO	0.00	-0.06	-0.06	-0.04
CHO	0.02	-0.04	-0.04	-0.01
CH ₂ O	-0.02	-0.03	-0.02	0.00
CH ₃ O	0.09	-0.07	-0.06	-0.04
CH ₃ OH	0.12	-0.10	-0.09	-0.05

1045

1046 Table 2: Energetics of adsorption-desorption reactions (in eV) for the HDO of guaiacol in the limit
 1047 of zero coverage at 473 K temperature under different reaction environments.

ID	Reaction	Vapor phase, ΔG_{rxn}	Water, ΔG_{rxn}	1-Butanol, ΔG_{rxn}	Diethyl ether, ΔG_{rxn}	n-Hexane, ΔG_{rxn}
1	$C_6H_4(OH)(OCH_3) \text{ (gas)} + 4^* \leftrightarrow C_6H_4(OH)(OCH_3) \text{ ****}$	-0.29	-0.51	-0.75	-0.72	-0.62
53	$C_6H_5(OCH_3) \text{ ****} \leftrightarrow C_6H_5(OCH_3) \text{ (gas)} + 4^*$	0.35	0.60	0.75	0.73	0.64
54	$C_6H_4(OH)_2 \text{ ****} \leftrightarrow C_6H_4(OH)_2 \text{ (gas)} + 4^*$	0.41	0.63	0.80	0.77	0.66
55	$C_6H_5OH \text{ ****} \leftrightarrow C_6H_5OH \text{ (gas)} + 4^*$	0.45	0.65	0.83	0.80	0.71
56	$C_6H_6 \text{ ***} \leftrightarrow C_6H_6 \text{ (gas)} + 3^*$	0.47	0.58	0.72	0.70	0.64
57	$CH_4^* \leftrightarrow CH_4 \text{ (gas)} + ^*$	-0.39	-0.43	-0.36	-0.36	-0.36
58	$CH_3OH^* \leftrightarrow CH_3OH \text{ (gas)} + ^*$	-0.38	-0.50	-0.28	-0.29	-0.33
59	$H_2O^* \leftrightarrow H_2O \text{ (gas)} + ^*$	-0.33	-0.34	-0.23	-0.24	-0.28
60	$CO^* \leftrightarrow CO \text{ (gas)} + ^*$	0.96	0.96	1.02	1.01	1.00
53	$H^* \leftrightarrow 0.5H_2 \text{ (gas)} + ^*$	0.18	0.22	0.19	0.19	0.19

1048

1049 Table 3. Energetics of all elementary surface reaction steps (in eV) for the HDO of guaiacol to
 1050 aromatics in the limit of zero coverage at 473 K in the presence of liquid water, 1-butanol, diethyl
 1051 ether, and n-hexane solvents.

ID	Reaction	Vapor phase		Water		1-Butanol		Diethyl ether		n-Hexane	
		ΔG_{rxn}	ΔG^\ddagger	ΔG_{rxn}	ΔG^\ddagger	ΔG_{rxn}	ΔG^\ddagger	ΔG_{rxn}	ΔG^\ddagger	ΔG_{rxn}	ΔG^\ddagger
2	$C_6H_4(OH)(OCH_3)^{****} + H^* \leftrightarrow C_6H_4H_\beta(OH)(OCH_3)^{****} + *$	0.40	1.10	0.41	1.12	0.49	1.27	0.48	1.28	0.47	1.25
3	$C_6H_4(OH)(OCH_3)^{****} + H^* \leftrightarrow C_6H_4H_\alpha(OH)(OCH_3)^{****} + *$	0.51	1.14	0.51	1.18	0.43	1.20	0.44	1.20	0.45	1.21
4	$C_6H_4(OH)(OCH_3)^{****} + * \leftrightarrow C_6H_4(OCH_3)^{****} + OH^*$	-0.22	1.06	-0.03	1.13	-0.13	1.06	-0.13	1.06	-0.12	1.07
5	$C_6H_4(OH)(OCH_3)^{****} + * \leftrightarrow C_6H_4OH^{****} + CH_3O^*$	-0.49	0.88	-0.37	0.95	-0.43	0.89	-0.42	0.90	-0.42	0.90
6	$C_6H_4(OH)(OCH_3)^{****} + 2* \leftrightarrow C_6H_4(OH)(OCH_2)^{*****} + H^*$	-0.36	0.50	-0.25	0.52	-0.32	0.51	-0.32	0.51	-0.32	0.51
7	$C_6H_4(OH)(OCH_3)^{****} + * \leftrightarrow C_6H_4(OH)(O)^{****} + CH_3^*$	-1.35	1.40	-1.23	1.43	-1.15	1.36	-1.15	1.37	-1.17	1.38
8	$C_6H_4(OH)(OCH_3)^{****} + * \leftrightarrow C_6H_4(O)(OCH_3)^{****} + H^*$	-0.77	0.29	-0.67	0.37	-0.65	0.29	-0.64	0.29	-0.65	0.31
9	$C_6H_4H_\beta(OH)(OCH_3)^{****} + 2* \leftrightarrow C_6H_4H_\beta(OH)(OCH_2)^{*****} + H^*$	-0.12	0.93	-0.27	0.81	-0.13	0.91	-0.12	0.92	-0.12	0.93
10	$C_6H_4H_\beta(OH)(OCH_3)^{****} + * \leftrightarrow C_6H_5OH^{****} + CH_3O^*$	-1.05	0.72	-0.97	0.61	-1.13	0.66	-1.12	0.67	-1.10	0.68
11	$C_6H_4H_\alpha(OH)(OCH_3)^{****} + * \leftrightarrow C_6H_5(OCH_3)^{****} + OH^*$	-0.91	0.57	-0.93	0.59	-0.81	0.70	-0.81	0.70	-0.81	0.68
12	$C_6H_4(OCH_3)^{****} + H^* \leftrightarrow C_6H_5(OCH_3)^{****} + *$	-0.18	0.64	-0.40	0.58	-0.25	0.55	-0.25	0.55	-0.24	0.56
13	$C_6H_4OH^{****} + H^* \leftrightarrow C_6H_5OH^{****} + *$	-0.16	0.62	-0.20	0.59	-0.22	0.61	-0.21	0.61	-0.21	0.60
14	$C_6H_4(OH)(OCH_2)^{*****} + * \leftrightarrow C_6H_4OH^{****} + CH_2O^{**}$	-0.25	1.23	-0.33	1.10	-0.19	1.34	-0.19	1.33	-0.18	1.32
15	$C_6H_4(OH)(OCH_2)^{*****} + * \leftrightarrow C_6H_4(O)(OCH_2)^{*****} + H^*$	-0.73	0.28	-0.69	0.31	-0.58	0.32	-0.58	0.32	-0.59	0.31
16	$C_6H_4(OH)(OCH_2)^{*****} + * \leftrightarrow C_6H_4(OH)(OCH)^{*****} + H^*$	-0.53	0.02	-0.52	0.00	-0.53	0.12	-0.53	0.12	-0.53	0.11
17	$C_6H_4(OH)(OCH_2)^{*****} \leftrightarrow C_6H_4(OH)(O)^{****} + CH_2^*$	-1.25	0.42	-1.30	0.43	-1.10	0.40	-1.10	0.40	-1.11	0.41
18	$C_6H_4(OH)(O)^{****} + H^* \leftrightarrow C_6H_4(OH)_2^{****} + *$	0.75	1.03	0.71	1.03	0.61	0.92	0.61	0.92	0.64	0.93
19	$C_6H_4(OH)(O)^{****} + H^* \leftrightarrow C_6H_4H_\alpha(OH)(O)^{****} + *$	0.89	1.40	0.87	1.47	0.86	1.37	0.86	1.37	0.85	1.38
20	$C_6H_4(OH)(O)^{****} + * \leftrightarrow C_6H_4O^{****} + OH^*$	0.51	1.15	0.72	1.11	0.41	1.14	0.42	1.14	0.45	1.15
21	$C_6H_4(O)(OCH_3)^{****} + * \leftrightarrow C_6H_4O^{****} + CH_3O^*$	0.21	1.08	0.32	1.04	0.16	1.15	0.17	1.16	0.19	1.16
22	$C_6H_4(O)(OCH_3)^{****} + 2* \leftrightarrow C_6H_4(O)(OCH_2)^{*****} + H^*$	-0.32	0.53	-0.27	0.47	-0.25	0.52	-0.25	0.51	-0.26	0.51
23	$C_6H_4H_\beta(OH)(OCH_2)^{*****} \leftrightarrow C_6H_4H_\beta(OH)(O)^{****} + CH_2^*$	-0.84	0.39	-0.65	0.55	-0.81	0.39	-0.80	0.40	-0.79	0.41
24	$C_6H_5(OCH_3)^{****} + * \leftrightarrow C_6H_5(OCH_2)^{****} + H^*$	-0.32	0.51	-0.20	0.52	-0.22	0.55	-0.21	0.56	-0.21	0.57

25	$C_6H_4(OH)(OCH)^{*****} + * \leftrightarrow C_6H_4OH^{*****} + CHO^{**}$	-0.26	1.00	-0.27	0.99	-0.20	0.95	-0.20	0.95	-0.20	0.95
26	$C_6H_4(OH)(OCH)^{*****} \leftrightarrow C_6H_4(OH)(O)^{****} + CH^*$	-1.29	0.31	-1.38	0.31	-1.12	0.32	-1.12	0.33	-1.13	0.34
27	$C_6H_4(OH)_2^{****} + * \leftrightarrow C_6H_4OH^{*****} + OH^*$	-0.16	1.16	-0.09	1.09	-0.13	1.16	-0.13	1.16	-0.13	1.15
28	$C_6H_4(OH)_2^{****} + H^* \leftrightarrow C_6H_5(OH)_2^{****} + *$	0.55	1.15	0.59	1.25	0.65	1.19	0.65	1.19	0.62	1.17
29	$C_6H_4H_6(OH)(O)^{****} + * \leftrightarrow C_6H_5O^{****} + OH^*$	-1.29	0.76	-1.20	0.74	-1.37	0.73	-1.36	0.73	-1.31	0.74
30	$C_6H_4O^{****} + H^* \leftrightarrow C_6H_5O^{****} + *$	-0.92	0.52	-1.04	0.43	-0.92	0.44	-0.91	0.45	-0.91	0.46
31	$C_6H_4(O)(OCH_2)^{*****} + * \leftrightarrow C_6H_4O^{****} + CH_2O^{**}$	0.40	1.03	0.46	1.01	0.32	1.02	0.32	1.02	0.34	1.01
32	$C_6H_4(O)(OCH_2)^{*****} + * \leftrightarrow C_6H_4O_2^{*****} + CH_2^*$	-0.95	0.52	-1.05	0.50	-1.02	0.51	-1.02	0.51	-1.01	0.50
33	$C_6H_4(O)(OCH_2)^{*****} + * \leftrightarrow C_6H_4(O)(OCH)^{*****} + H^*$	-0.52	0.02	-0.52	0.02	-0.57	0.00	-0.57	0.00	-0.58	0.00
34	$C_6H_4(O)(OCH)^{*****} + * \leftrightarrow C_6H_4O_2^{*****} + CH^*$	-1.00	0.50	-1.13	0.52	-1.02	0.51	-1.01	0.53	-0.98	0.54
35	$C_6H_4(O)(OCH)^{*****} + * \leftrightarrow C_6H_4(O)(OC)^{*****} + H^*$	-0.34	0.40	-0.39	0.41	-0.31	0.45	-0.30	0.46	-0.29	0.47
36	$C_6H_4H_6(OH)(O)^{****} + H^* \leftrightarrow C_6H_5(OH)_2^{****} + *$	0.25	0.91	0.26	0.94	0.29	0.92	0.28	0.92	0.27	0.92
37	$C_6H_5(OCH_2)^{****} + * \leftrightarrow C_6H_5O^{****} + CH_2^*$	-1.30	0.18	-1.24	0.16	-1.32	0.24	-1.32	0.23	-1.31	0.23
38	$C_6H_5O^{****} + H^* \leftrightarrow C_6H_5OH^{****} + *$	0.84	1.03	0.73	1.00	0.77	1.04	0.76	1.04	0.77	1.03
39	$C_6H_5OH^{****} + * \leftrightarrow C_6H_5^{****} + OH^*$	-0.10	1.17	-0.01	1.09	-0.07	1.21	-0.06	1.21	-0.05	1.20
40	$C_6H_5OH^{****} + H^* \leftrightarrow C_6H_6OH^{****} + *$	0.59	1.25	0.53	1.21	0.67	1.34	0.67	1.34	0.67	1.33
41	$C_6H_5(OH)_2^{****} + * \leftrightarrow C_6H_5OH^{****} + OH^*$	-0.87	0.56	-0.89	0.57	-0.99	0.41	-0.99	0.41	-0.95	0.45
42	$C_6H_4O_2^{*****} + H^* \leftrightarrow C_6H_4(OH)(O)^{****} + 2^*$	0.43	0.95	0.44	0.97	0.50	0.95	0.51	0.95	0.50	0.95
43	$C_6H_4(O)(OC)^{*****} \leftrightarrow C_6H_4O^{****} + CO^*$	-0.49	0.66	-0.28	0.70	-0.57	0.69	-0.57	0.70	-0.55	0.69
44	$C_6H_5^{****} + H^* \leftrightarrow C_6H_6^{***} + 2^*$	-0.20	0.54	-0.21	0.56	-0.15	0.53	-0.15	0.54	-0.17	0.55
45	$C_6H_6OH^{****} \leftrightarrow C_6H_6^{***} + OH^*$	-0.89	0.53	-0.74	0.59	-0.88	0.55	-0.89	0.54	-0.88	0.54
46	$CH^* + H^* \leftrightarrow CH_2^* + *$	0.57	0.61	0.60	0.60	0.56	0.56	0.56	0.56	0.56	0.57
47	$CH_2^* + H^* \leftrightarrow CH_3^* + *$	0.27	0.62	0.31	0.61	0.26	0.57	0.26	0.58	0.26	0.58
48	$CH_3^* + H^* \leftrightarrow CH_4^* + *$	0.43	1.03	0.32	1.08	0.40	0.98	0.39	0.99	0.40	1.00
49	$OH^* + H^* \leftrightarrow H_2O^* + *$	0.48	1.13	0.41	1.04	0.39	1.11	0.40	1.11	0.42	1.12
50	$CHO^{**} + H^* \leftrightarrow CH_2O^{**} + *$	0.54	0.51	0.46	0.48	0.54	0.50	0.55	0.50	0.54	0.50
51	$CH_2O^{**} + H^* \leftrightarrow CH_3O^* + 2^*$	0.13	0.69	0.21	0.71	0.08	0.68	0.08	0.67	0.08	0.67
52	$CH_3O^* + H^* \leftrightarrow CH_3OH^* + *$	0.71	1.21	0.69	1.16	0.67	1.23	0.67	1.23	0.69	1.23

1052

1053

1054 Table 4: Computed overall turnover frequencies at various reaction temperatures and 15 bar partial
1055 pressure of hydrogen for the HDO of guaiacol over a Ru(0001) surface. Microkinetic models have
1056 been simulated for 1% conversion of guaiacol using 0.5 g guaiacol in 10 g of various solvent
1057 media. For vapor phase simulations, we used a guaiacol chemical potential corresponding to the
1058 one in liquid water.

TOF (s ⁻¹)	Temperature			
	423 K	473 K	523 K	573 K
Vapor phase	6.46×10^{-7}	1.95×10^{-4}	4.31×10^{-2}	2.35
Water	1.54×10^{-7}	6.70×10^{-5}	3.25×10^{-2}	4.82×10^{-1}
1-Butanol	4.64×10^{-6}	4.66×10^{-4}	1.76×10^{-2}	3.08×10^{-1}
Diethyl ether	4.07×10^{-6}	4.33×10^{-4}	1.80×10^{-2}	2.98×10^{-1}
n-Hexane	4.94×10^{-6}	5.17×10^{-4}	2.34×10^{-2}	4.14×10^{-1}

1059

1060 Table 5. Coverages (%) of most abundant surface intermediates in various reaction environments
1061 for the HDO of guaiacol at 473K.

Surface Intermediates	Vapor phase	Water	1-Butanol	Diethyl ether	n-Hexane
θ^*	0.13	0.10	0.39	0.41	0.35
θ_H^*	7.04	11.73	11.42	11.49	11.03
θ_{CO}^*	28.17	25.78	29.96	30.09	29.65
θ_{CH}^*	62.75	60.20	0.03	0.05	0.34
$\theta_{C_6H_4O_2}^*$	0.65	0.10	46.7	48.45	51.20
$\theta_{Phenoxy}^*$	0.76	1.84	9.72	8.24	5.68

1062

1063 Table 6. Kinetic parameters computed at 473 K for the HDO of guaiacol over a Ru(0001) model
 1064 surface at low conversion conditions in various reaction environments.

Properties	Partial pressure (bar)	Vapor phase	Water	1-Butanol	Diethyl ether	n-Hexane
Apparent Activation Energy(eV)	-	2.12	2.15	1.55	1.57	1.58
Guaiacol order	0.20 - 10.0	0.17	0.20	0.12	0.12	0.12
Carbon monoxide order	1.0×10^{-5} - 1.0×10^{-1}	-0.51	-0.65	-0.18	-0.18	-0.18
Hydrogen order	0.20 - 0.40	-1.18	-4.02	0.68	0.59	0.43
	0.60-20.0	1.74	1.62	0.46	0.46	0.44

1065

1066 Table 7. Thermodynamic and kinetic sensitivity analysis at 473 K for the HDO of guaiacol over
 1067 a Ru(0001) model surface.

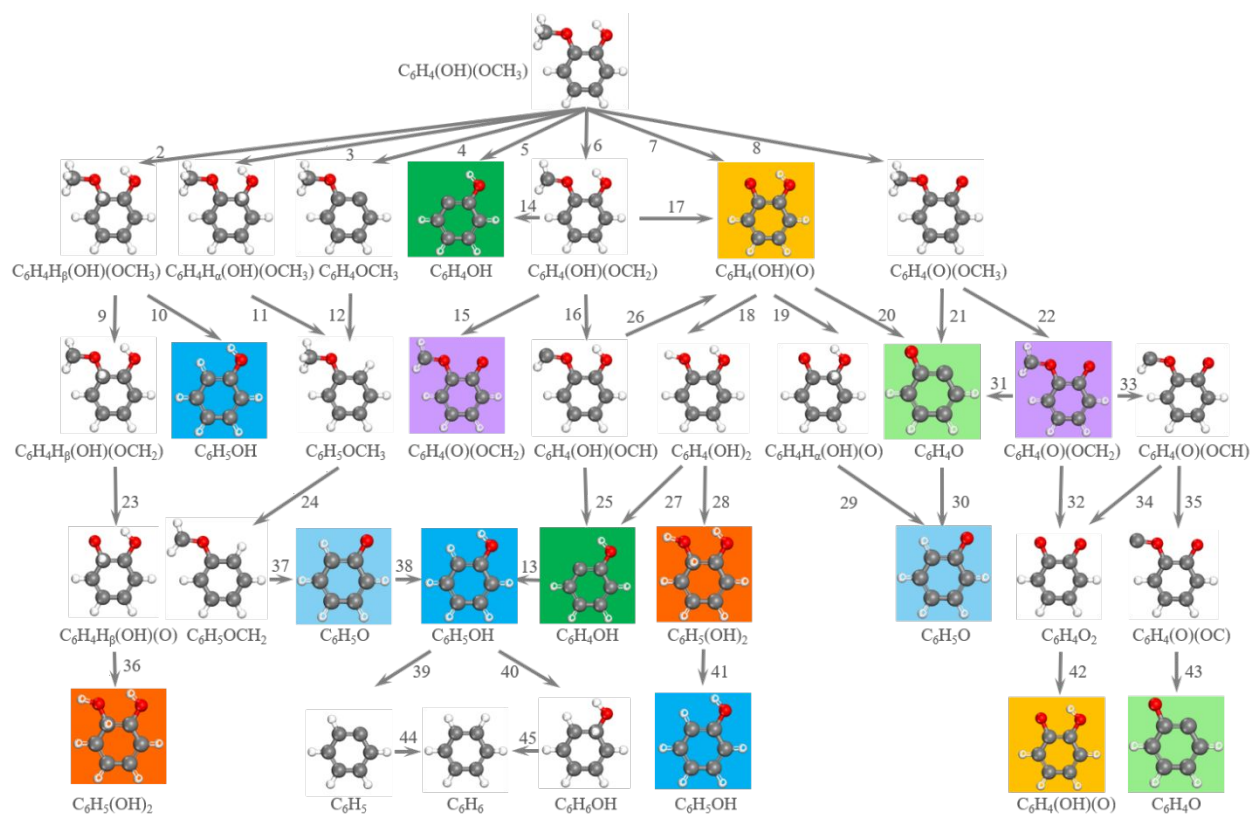
Degree of thermodynamic rate control					
Species	Vapor	Water	1-Butanol	Diethyl ether	n-Hexane
H*	-0.94	-0.35	-0.60	-0.66	-0.55
CO*	-0.63	-0.79	-0.18	-0.20	-0.21
CH*	-0.90	-0.86	0.00	0.00	0.00
C ₆ H ₄ O ₂ *****	-0.01	0.00	-0.80	-0.82	-0.82
Degree of kinetic rate control					
C ₆ H ₄ (OH)(OCH ₃) (gas) + 4* ↔ C ₆ H ₄ (OH)(OCH ₃)*****	0.15	0.20	0.16	0.16	0.16
C ₆ H ₄ (OH)(O)***** + * ↔ C ₆ H ₄ O***** + OH*	-0.01	0.01	0.77	0.80	0.82
C ₆ H ₄ (O)(OCH)***** + * ↔ C ₆ H ₄ O ₂ ***** + CH*	-0.72	-0.75	-0.60	-0.61	-0.64
C ₆ H ₄ (O)(OCH)***** + * ↔ C ₆ H ₄ (O)(OC)***** + H*	0.74	0.73	0.57	0.58	0.61
CH ₃ * + H* ↔ CH ₄ * + *	0.84	0.86	0.00	0.00	0.01

1068

1069 Table 8. Energetics of important elementary surface reaction steps (in eV) in the limit of zero
 1070 coverage at 473 K in the presence of liquid water, 1-butanol, diethyl ether, and n-hexane solvents
 1071 for the phenol hydrogenation to cyclohexanol. Condensed phase effects have not been computed
 1072 for reactions 1, 37, 52, and 77 due to their high activation barriers in vapor phase in comparison to
 1073 the alternate route reaction 80.

ID	Reaction	Vapor phase		Water		1-Burtanol		Diethyl ether		n-Hexane	
		ΔG_{rxn}	ΔG^\ddagger	ΔG_{rxn}	ΔG^\ddagger	ΔG_{rxn}	ΔG^\ddagger	ΔG_{rxn}	ΔG^\ddagger	ΔG_{rxn}	ΔG^\ddagger
1	Phenol**** + H* \leftrightarrow HC1-1**** + *	0.41	1.16	N/A	N/A	N/A	N/A	N/A	N/A	N/A	N/A
37	Phenol**** + H* \leftrightarrow HC2-1**** + *	0.58	1.11	N/A	N/A	N/A	N/A	N/A	N/A	N/A	N/A
52	Phenol**** + H* \leftrightarrow HC3-1**** + *	0.51	1.05	N/A	N/A	N/A	N/A	N/A	N/A	N/A	N/A
77	Phenol**** + H* \leftrightarrow HC4-1**** + *	0.71	1.15	N/A	N/A	N/A	N/A	N/A	N/A	N/A	N/A
80	Phenol**** + * \leftrightarrow KET-1**** + H*	-0.76	0.31	-0.77	0.34	-0.75	0.32	-0.75	0.32	-0.75	0.31
92	KET-4b**** + H* \leftrightarrow KET-5c**** + *	0.17	1.07	0.12	0.90	0.10	0.97	0.10	0.98	0.10	0.99
96	KET-5c**** + H* \leftrightarrow KET-6**** + *	0.32	1.21	0.23	1.04	0.24	1.15	0.24	1.17	0.24	1.18
98	KET-6**** + H* \leftrightarrow KET-7a**** + *	0.60	1.22	0.57	1.17	0.59	1.24	0.59	1.25	0.59	1.26
100	KET-7a**** + H* \leftrightarrow HC-6**** + *	-0.11	1.17	-0.13	1.09	-0.14	1.10	-0.13	1.11	-0.13	1.11
102	KET-1**** + H* \leftrightarrow KET-2b**** + *	0.94	1.14	0.90	1.21	0.90	1.14	0.90	1.13	0.90	1.12
105	KET-2b**** + H* \leftrightarrow KET-3g**** + *	0.27	0.84	0.24	0.86	0.23	0.81	0.23	0.80	0.23	0.80
109	KET-3g**** + H* \leftrightarrow KET-4d**** (=KET-4b****) + *	0.42	1.06	0.44	0.93	0.44	0.95	0.44	0.96	0.43	1.02

1074

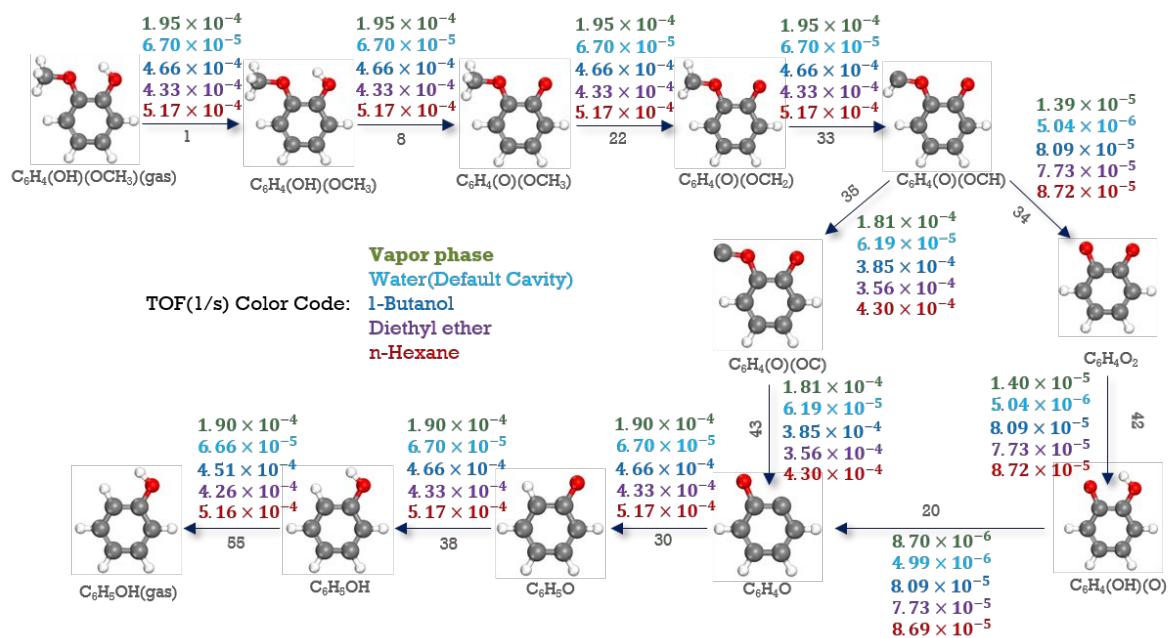


1075

1076 Figure 1: Reaction network investigated for the hydrodeoxygenation of guaiacol over a Ru(0001)

1077 model surface. Duplicate structures are highlighted by identical background colors.

1078

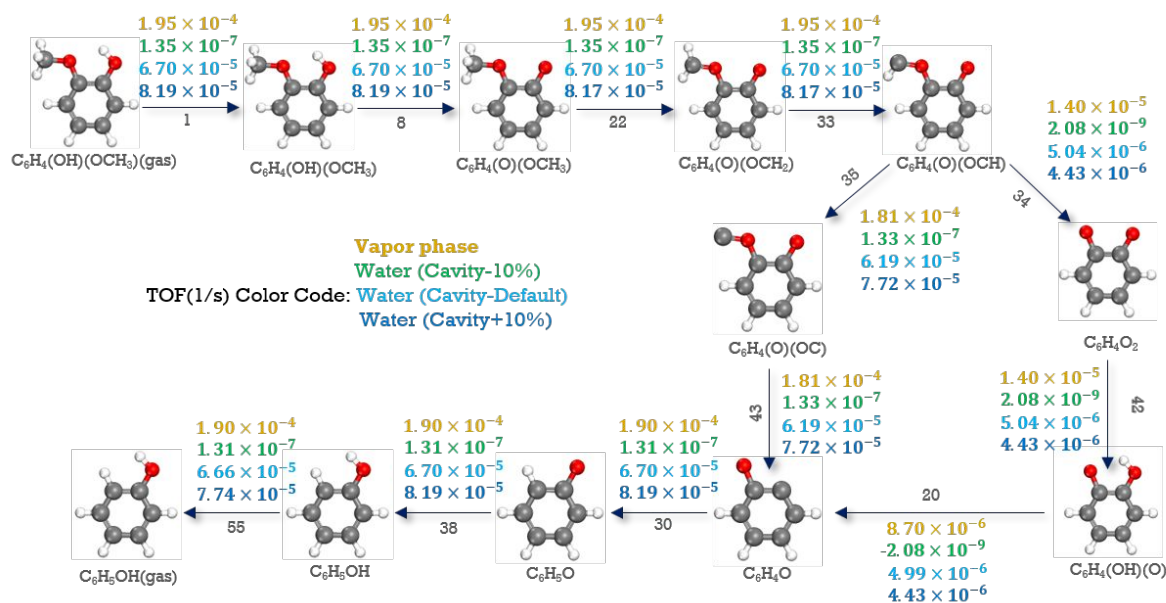


1079

1080 Figure 2: Turnover frequencies (1/s) along the dominant reaction pathway for the HDO of guaiacol

1081 to aromatic products over a Ru(0001) surface computed in different reaction environments.

1082



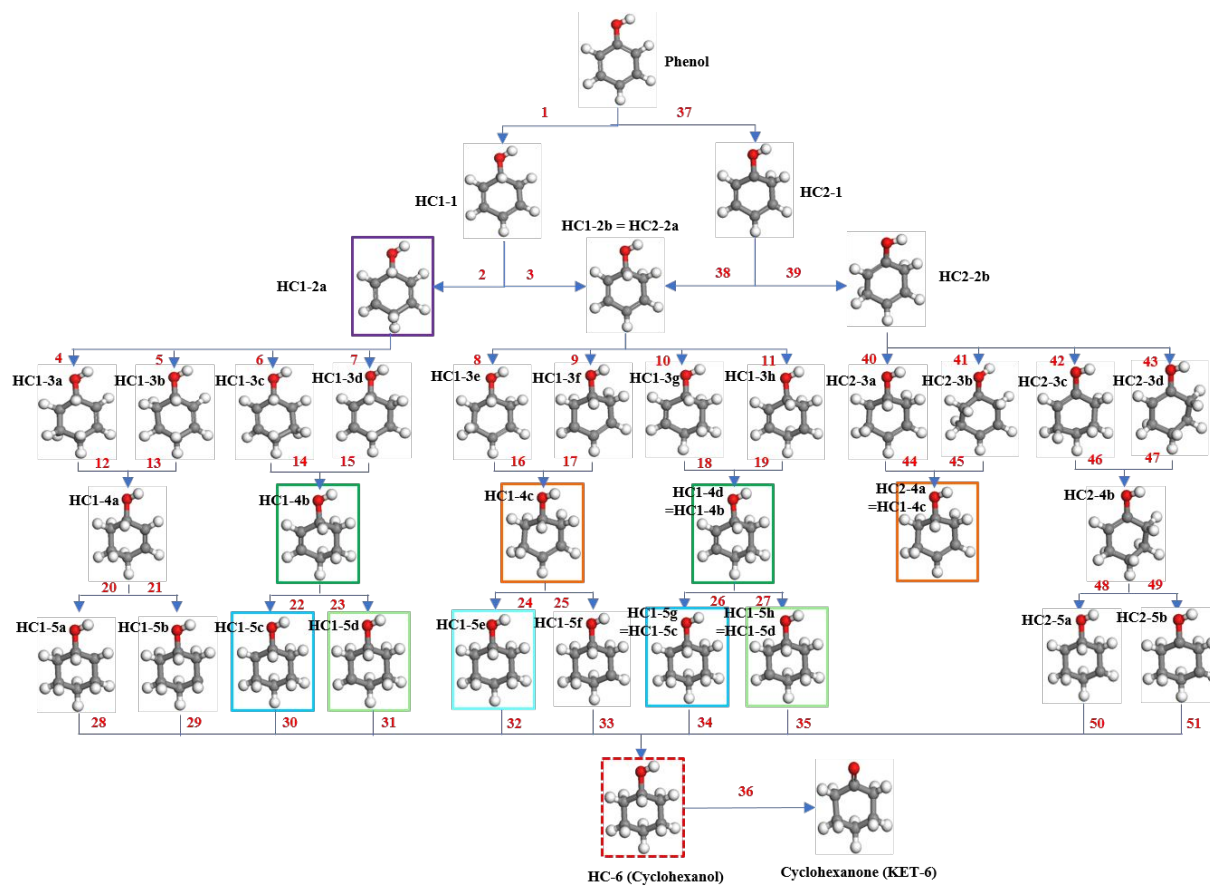
1083

1084 Figure 3: Turnover frequencies (1/s) along the dominant reaction pathway for the HDO of guaiacol

1085 to aromatic products over a Ru(0001) surface in vapor and aqueous phases. Aqueous phase

1086 calculations have been performed using three different cavity radius of Ru atoms.

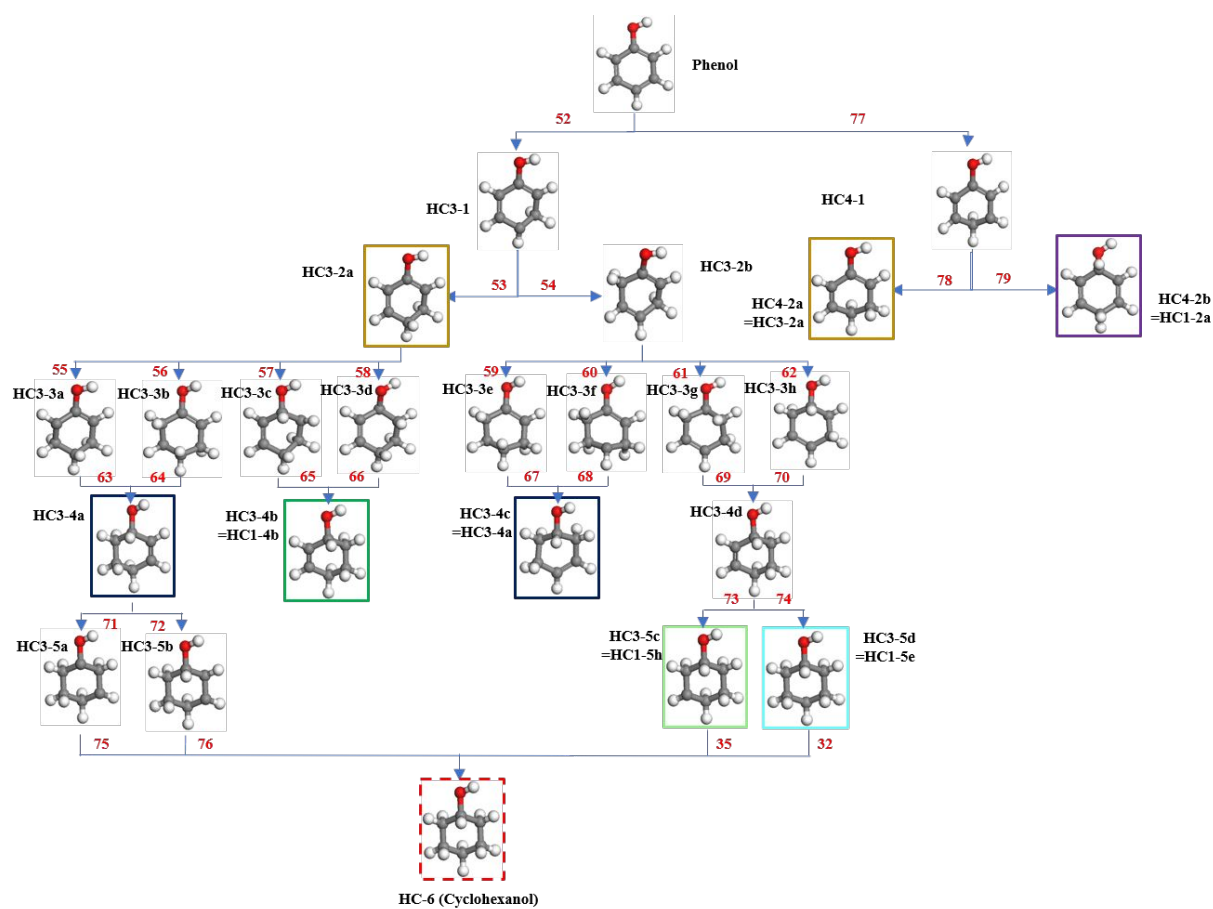
1087



1088

1089 Figure 4: Reaction network investigated along the C₁ and C₂ hydrogenation pathway of phenol
 1090 over a Ru(0001) model surface. Duplicate structures have been highlighted by identical border
 1091 colors.

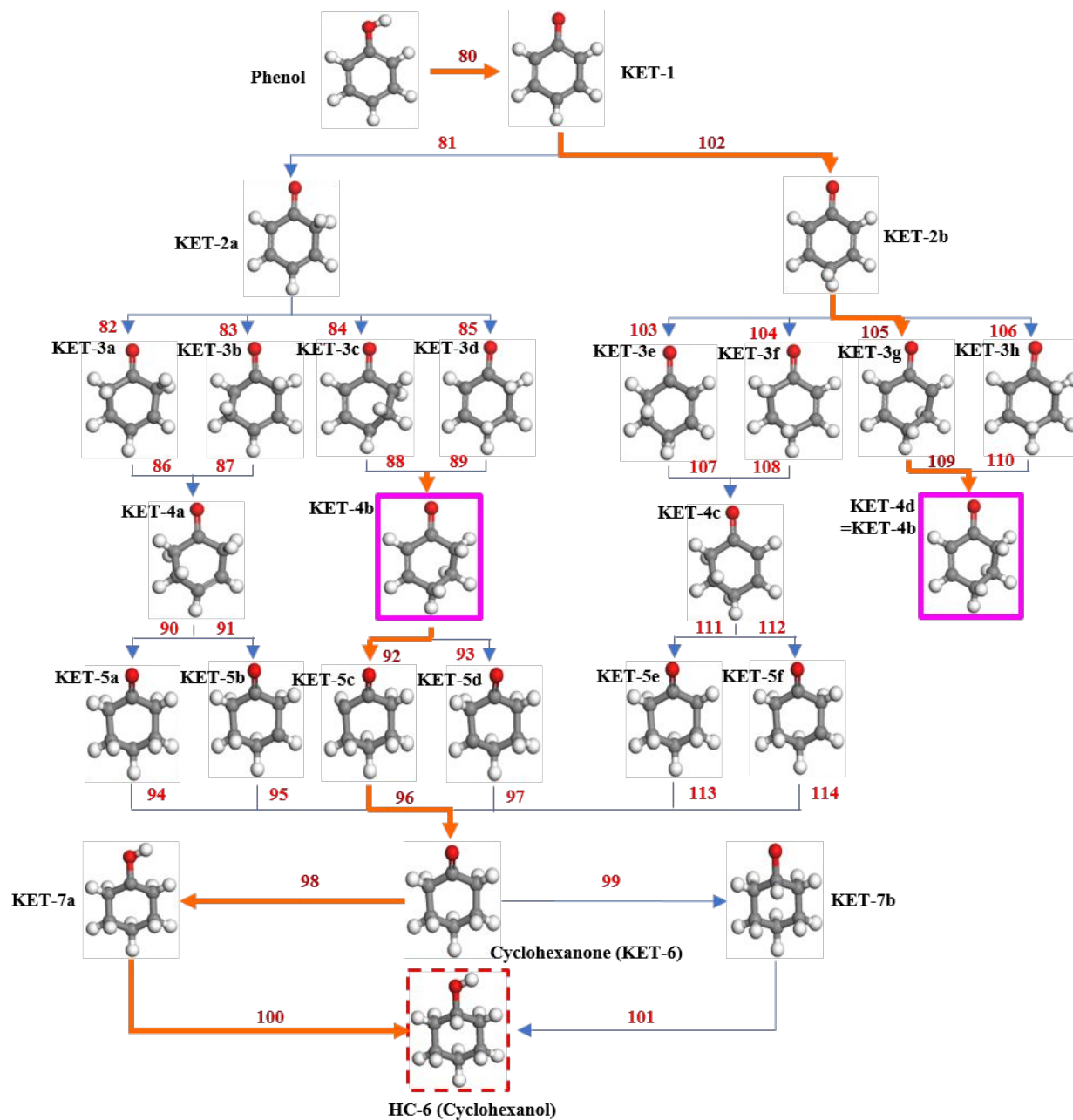
1092



1093

1094 Figure 5: Reaction network investigated along the C₃ and C₄ hydrogenation pathway of phenol
 1095 over a Ru(0001) model surface. Duplicate structures have been highlighted by identical border
 1096 colors.

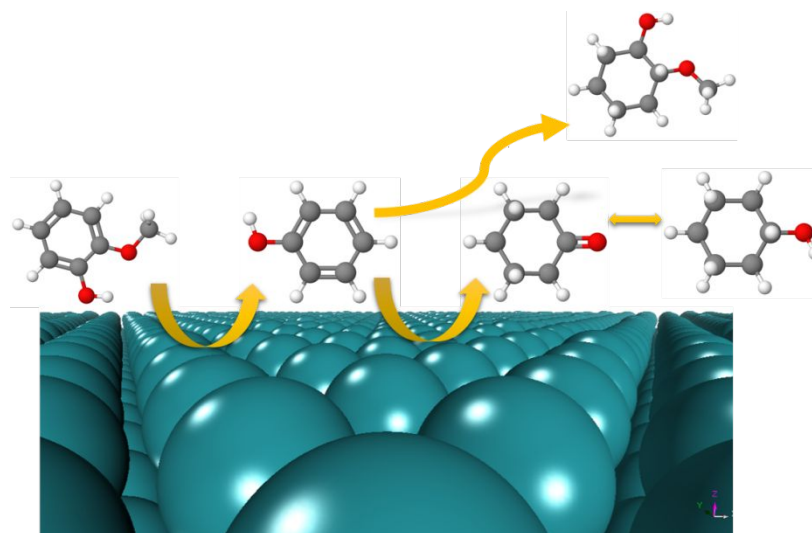
1097



1098

1099 Figure 6: Reaction network investigated along the keto-enol tautomerization pathway of phenol
 1100 over a Ru(0001) model surface. Duplicate structures have been highlighted by identical border
 1101 colors. Proposed reaction mechanism and the reaction steps involved in the cycloalkane production
 1102 from phenol have also been highlighted.

1103



1104

1105

TOC